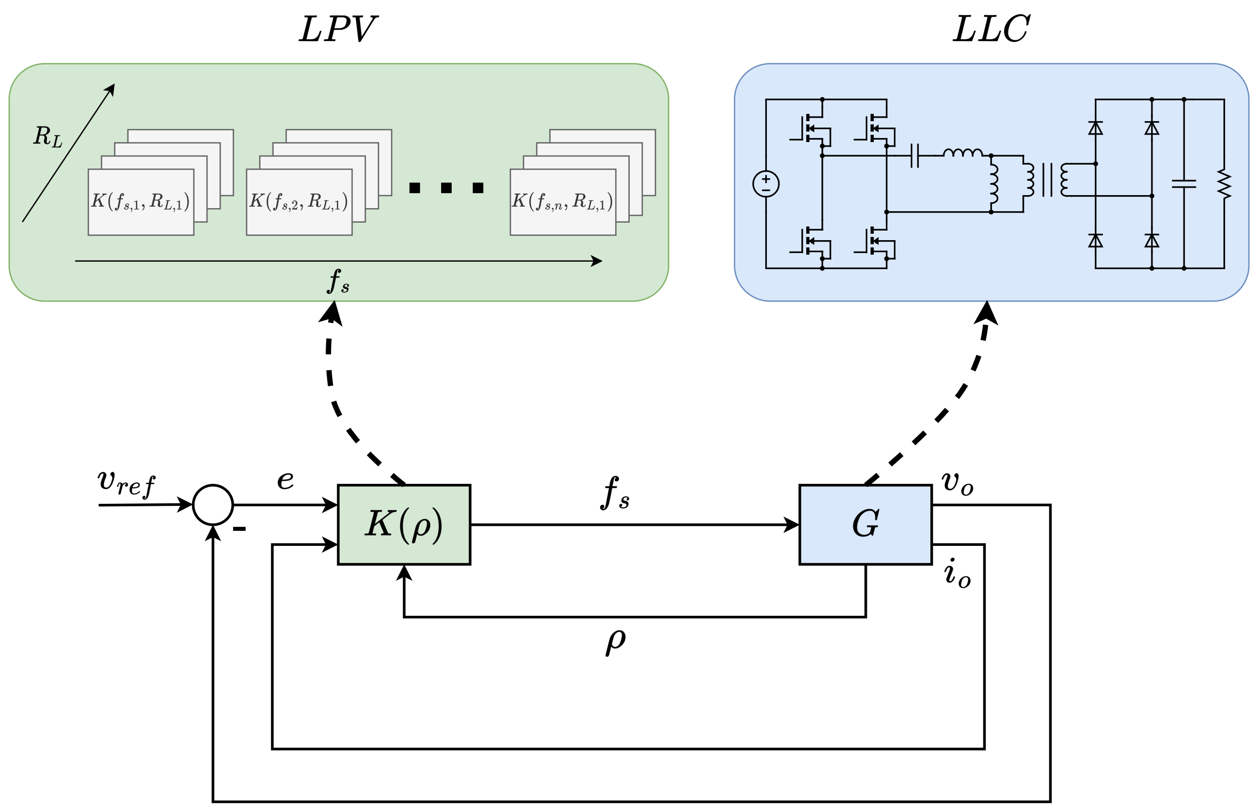

Parameter scheduled robust MIMO DC-DC converter control

Frequency scheduled wide range LLC DC-DC converter control - a robust LPV MIMO approach

Master's thesis in System, Controls & Mechatronics

Daniel Quach

DEPARTMENT OF ELECTRICAL ENGINEERING

CHALMERS UNIVERSITY OF TECHNOLOGY
Gothenburg, Sweden 2023
www.chalmers.se

Master's thesis 2023

Parameter scheduled robust MIMO DC-DC converter control

Frequency scheduled wide range LLC DC-DC converter control
- a robust LPV MIMO approach

Daniel Quach

CHALMERS
UNIVERSITY OF TECHNOLOGY

Department of Electrical Engineering
Division of Systems and Control
Automatic Control Group
Chalmers University of Technology
Gothenburg, Sweden 2023

Parameter scheduled robust MIMO DC-DC converter control
Frequency scheduled wide range LLC DC-DC converter control
- a robust LPV MIMO approach
Daniel Quach

Supervisor: Spyros Gryparis, Aros Electronics & Mebtu Beza, E2
Examiner: Balázs Adam Kulcsár, AC, E2

Master's Thesis 2023
Department of Electrical Engineering
Division of Systems and Control
Automatic Control group
Chalmers University of Technology
SE-412 96 Gothenburg
Telephone +46 31 772 1000

Cover: System block diagram overview with LPV controller

Typeset in LaTeX
Printed by Chalmers Reproservice
Gothenburg, Sweden 2023

Parameter scheduled robust MIMO DC-DC converter control
Frequency scheduled wide range LLC DC-DC converter control
- a robust LPV MIMO approach
Daniel Quach
Department of Electrical Engineering
Chalmers University of Technology

Abstract

This project presents the design and evaluation of different controller strategies for voltage regulation of a resonant LLC DC-DC converter. The controllers evaluated include the classical proportional and integral controllers, as well as the more robust model-based control methods. To handle the nonlinear characteristics of the converter, the project also explored gain scheduled, and linear parameter-varying control methods using an affine state-space representation derived from existing converter models. Robustness was evaluated by simulating the disturbance rejection capabilities of the controllers. The results show that while the robust control methods provided increased robustness for a larger operating range, they also resulted in overly conservative controllers for certain operating conditions. The LPV controller managed to improve robustness throughout the whole operating range without affecting controller response times, emphasizing the importance of including nonlinearity in the control design for this type of converter.

Keywords: LPV, robust control, gain scheduling, DC-DC, LLC, resonant converter, MIMO.

Acknowledgements

This project would not have been possible without the help and guidance of various individuals. First and foremost, I would like to express my deepest gratitude to my examiner, Prof. Balázs Adam Kulcsár, for his expert advice and valuable insights throughout the entire project.

Secondly, many thanks to my supervisors, Spyros Gryparis, Oskar Theliander, and Mebtu Beza. Their deep knowledge of power electronics has been extremely helpful in improving the depth and quality of the project.

Lastly, I would like to extend my thanks to Aros Electronics for providing me with the opportunity to undertake this project.

Daniel Quach, Gothenburg, June 2023

List of Acronyms

Below is the list of acronyms that have been used throughout this thesis listed in alphabetical order:

AC	**A**lternating **C**urrent
DC	**D**irect **C**urrent
PWM	**P**ulse-**W**idth-**M**odulation
ZVS	**Z**ero **V**oltage **S**witching
ZCS	**Z**ero **C**urrent **S**witching
FHA	**F**undamental **H**armonic **A**nalysis
LPV	**L**inear **P**arameter-**V**arying
EDF	**E**xtended **D**escribing **F**unction
SISO	**S**ingle-**I**nput **S**ingle-**O**utput
MIMO	**M**ultiple-**I**nput **M**ultiple-**O**utput
PID	**P**roportional-**I**ntegral-**D**erivative
PI	**P**roportional-**I**ntegral

Nomenclature

Below is the nomenclature of parameters and variables that have been used throughout this thesis.

Parameters

V_{in}	Input voltage
V_o	Output voltage
L_r	Resonant inductance (series)
C_r	Resonant capacitance (series)
L_m	Magnetizing inductance (parallel)
C_o	Output capacitance
L_{rp}	Perturbed resonant inductance (series)
C_{rp}	Perturbed resonant capacitance (series)
L_{mp}	Perturbed magnetizing inductance (parallel)
C_{op}	Perturbed output capacitance
R_L	Output resistance (load)
n	Transformer turns ratio
R_{ac}	Reflected load resistance
K	Resonant tank voltage gain
k_f	Small-signal voltage gain
L_{eq}	Equivalent tank inductance
f_r	Resonance frequency (Hz)
w_s	Resonance frequency (rad/s)
f_s	Switching frequency
F	Normalized switching frequency $\frac{f_s}{f_r}$
Q	Load factor
m	Inductance ratio

ζ	Damping ratio
K_p	Proportional gain
K_i	Integral gain
K_d	Derivative gain
A	State matrix
B	Input matrix
$\bar{E}$	LPV offset matrix
W	Performance output weight

Variables

$\dot{x}$	State derivatives
x	State vector
u	Input vector
y	Output vector
$\bar{x}$	State equilibrum points
$\bar{u}$	Input equilibrum points
$\Delta\dot{x}$	Linearized state derivatives $(\dot{x} - \dot{\bar{x}})$
Δx	Linearized state vector $(x - \bar{x})$
Δu	Linearized input vector $(u - \bar{u})$
ρ	Scheduling parameter
z	Performance output
d	Disturbance
e	Error signal
K	Controller
G	Plant
P	Generalized plant
$p,\ p^*$	Dominant pole pair
i_{Lr}	Resonant inductor current
i_{Lm}	Magnetizing inductor current
v_c	Resonant capacitor voltage
i_o	Output current
v_o	Output voltage
i_{rs}	Resonant inductor current - sine component

i_{rc}	Resonant inductor current - cosine component
v_{cs}	Resonant capacitor voltage - sine component
v_{cc}	Resonant capacitor voltage - cosine component
i_{ms}	Magnetizing inductor current - sine component
i_{mc}	Magnetizing inductor current - cosine component
i_p	Primary side transformer current
G_{if}	Frequency-to-current transfer function
G_{vi}	Current-to-voltage transfer function
G_{cl}	Inner closed-loop transfer function
C_i	Current controller transfer function (inner)
C_v	Voltage controller transfer function (outer)

Contents

List of Figures

List of Tables

1 Introduction

Power converters can be found in nearly all modern power systems. They are electronic devices that enable electrical energy to be converted between different electrical systems. The power level of a converter can vary depending on the application, ranging from low-power embedded systems to high-power chargers for electric vehicles. Recently, efficient and reliable DC-DC converters have become increasingly important as the number of systems using DC have grown. Particularly, the ongoing electrification of vehicles has created a need for DC-DC conversion in battery-based systems and chargers.

1.1 Background

LLC resonant converters have become popular recently due to their high efficiency (resonant switching), fast switching speeds, and high power density. However, LLC converters also present some difficulties in terms of modeling and control. Compared to the PWM-based converters, the LLC converter is highly nonlinear with different operation modes [2]. Thus, the traditional modeling techniques employed in PWM converters cannot be applied to LLC converters.

The currently existing control methods for LLC converters are mainly limited to simple single-input, single-output (SISO) approaches [1]. These simple controller structures do not consider the coupled dynamics between the different inputs and outputs. The field of control design for LLC converters is relatively new and few model-based multiple-input, multiple-output (MIMO) approaches have been explored so far. These model-based approaches are often more effective as they take into account the coupled dynamics through the system model [3]. Hence, there is a need to explore and develop model-based control methods that can effectively handle the complexity and nonlinearity of LLC converters in a MIMO framework.

This thesis aims to provide a comprehensive study of different control algorithms for LLC converters and their performance, with a focus on disturbance and uncertainty rejection. Through this project, the goal is to investigate and evaluate control techniques that can improve the performance and reliability of LLC converters.

1.2 Objective & Scope

The main objective of this project is to explore and develop control algorithms that can handle the nonlinear characteristics of LLC converters. Specifically, the focus is on achieving reliable operation across the whole operating range of the converter.

The scope of the project is defined as:

- Converter modeling
  - Investigate the nonlinear behavior and operating regions of LLC converters.
  - Derive a linear analytical model of the converter.
  - Evaluate the model accuracy and suitability for state feedback control design.

- Controller design
  - Design and implement controllers based on the derived model.
  - Explore robust control methods to improve disturbance and uncertainty rejection.
  - Explore scheduled controllers to improve controller response for nonlinear dynamics.

- Controller evaluation
  - Simulate the closed-loop system for model uncertainty and different disturbances.
  - Compute performance metrics for the simulations to relate design parameters to controller performance.

1.3 Limitations

- The thesis will exclude certain design parameters of the LLC DC-DC converter to focus on the control aspects of the converter. Thus, the type of transformer and power switches used will not be discussed.

- The simulations will be limited to certain load types, mainly resistive loads in conjunction with the capacitive output filter. Fully capacitive loads will be excluded, as they are far less common in many practical systems.

- Practical implementation of the controllers will not be extensively covered in this project. The focus of the project is on the theoretical development and evaluation of the controllers.

1.4 Ethics & Sustainability

The use of LLC converters can bring advantages in terms of sustainability. LLC converters have demonstrated higher power efficiency than traditional DC-DC converters with comparable production costs [4].

Additionally, the use of robust control methods can compensate for component value variations and degradation, which in turn can improve the lifespan and reliability of the converter. Therefore, the risk of accidents due to converter failure can be decreased, increasing the safety of workplaces. This can also help to reduce the need for frequent maintenance and replacements.

2

Theory

2.1 Resonant Converters

A resonant converter consists of four main stages. The first stage is a switch network which produces a square wave voltage from a DC source. The square wave voltage is then passed through a resonant tank stage, which produces a sinusoidal current. The magnitude of the current can be controlled by adjusting the switching frequency of the input square wave. The sinusoidal current is finally rectified and filtered by the rectifier and output filter stages, respectively. In many cases, a voltage transformer is also added between the resonant tank and rectifier for additional scaling of the output voltage and current. A general block diagram of a resonant converter is shown in Fig 2.1.

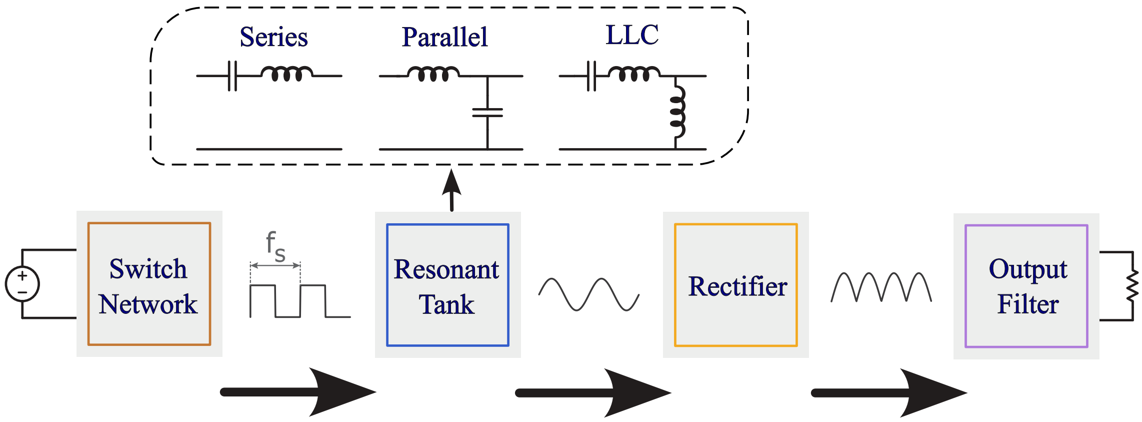

Figure 2.1: General block diagram for LLC converter stages. Modified from [1].

The resonant tank is the key component that provides the main advantages of a resonant converter. The resonant tank has a simple circuit topology, making the required component count comparable to traditional switched-mode converters [5]. The higher operating frequencies also reduce the size of the inductive components. Overall, this results in a high power density. The resonant tank plays a critical role in the efficiency of the converter as well. By using resonance, the converter can switch at zero voltage (ZVS) and zero current (ZCS) for certain operating conditions, reducing the switching losses and increasing the efficiency of power conversion. The resonant tank can have different configurations, which give different gain characteristics for the converter. The most common configurations are the series resonant tank, the parallel resonant tank, and the LLC tank. As explained in [6], both the series and parallel topologies have drawbacks that limit their effectiveness in a practical setting. The series topology has a low range of voltage regulation during light loads, while the parallel topology suffers from poor efficiency when stepping down voltages [6].

2.1.1 LLC Converter

The LLC resonant converter solves these issues by combining both topologies in the resonant tank. Another practical advantage of the LLC converter is that the inductive components can easily be integrated into the voltage transformer, reducing size and cost. As mentioned in [5], the leakage inductance of a non-ideal transformer can be used as an inductive component for the LLC tank. The LLC converter has a resonant tank that is composed of one series capacitor C_r, one series inductor L_r, and one parallel inductor L_m.

The gain characteristics for the LLC converter are derived through fundamental harmonic analysis (FHA) of the resonant tank. By only considering the fundamental harmonic of the input square wave, AC circuit analysis can be applied to obtain the transfer function. For configurations with a transformer, the load on the secondary side can be represented with an equivalent reflected load on the primary side, as shown in Fig 2.2.

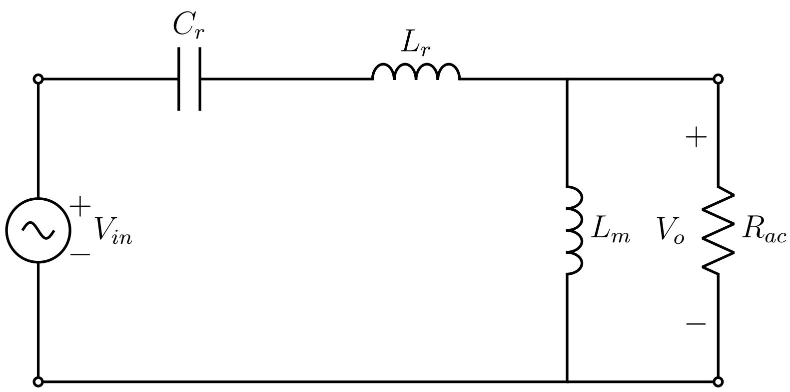

Figure 2.2: Equivalent resonant tank with reflected load.

As discussed in [2], the voltage gain can then be derived as (2.1)-(2.2).

$$K(F, R_L) = \left|\frac{V_o}{V_{in}}\right| = \frac{F^2(m-1)}{\sqrt{(m \cdot F^2 - 1)^2 + F^2(F^2-1)^2(m-1)^2Q^2}} \tag{2.1}$$

For clarity, the voltage gain is expressed with its normalized frequency F, the load factor Q, and the inductance ratio m defined in (2.2).

$$Q = \frac{\sqrt{L_r/C_r}}{R_{ac}}, \qquad R_{ac} = \frac{8}{\pi^2}n^2R_L, \qquad m = \frac{L_r + L_m}{L_r}, \qquad F = \frac{f_s}{f_r}, \tag{2.2}$$

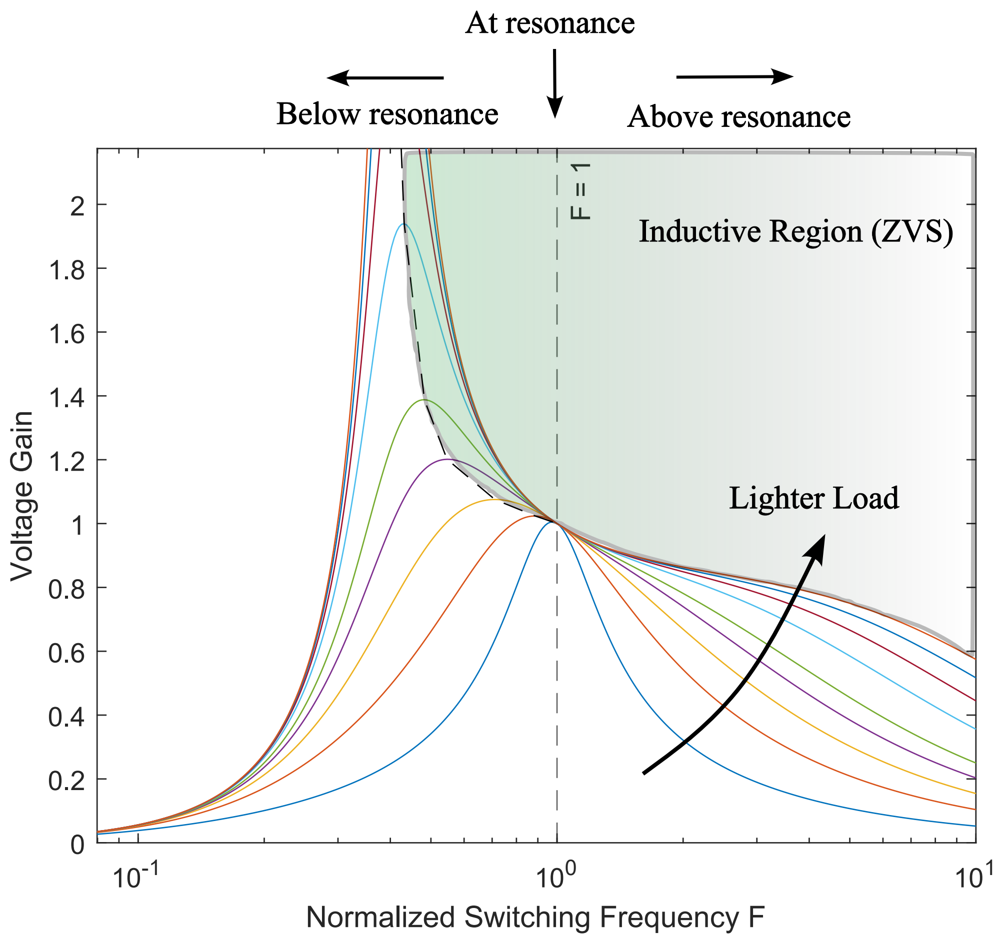

Figure 2.3: Voltage gain characteristics K for the LLC converter.

As observed, the voltage gain of the LLC converter is dependent on both the switching frequency (control input) and the output load (disturbance). From the circuit analysis, it also is possible to identify different impedance regions for the converter. The capacitive region indicates where the tank impedance has a capacitive nature. This region should be avoided as ZVS cannot be achieved here, lowering the power efficiency. To achieve ZVS, the converter has to operate in the inductive region [2].

Additionally, the LLC converter can also be divided into different operating regions based on switching frequency, as discussed in [2].

- Below resonance, $F < 1$
- At resonance, $F = 1$
- Above resonance, $F > 1$

The nominal operating point is typically set to be at resonance. The tank impedance is near zero at this frequency, meaning that the power efficiency is at its highest.

When operating in the different regions, the tank impedance and operating cycle of the LLC converter change, resulting in varying dynamics [2]. Consequently, designing a controller for the LLC converter is not simple, as it must consider the different dynamics and voltage gains across the whole operating range.

2.2 LLC Resonant Converter Modeling

The LLC converter can be described by the following nonlinear differential equations, as discussed in [6].

$$\frac{di_{Lr}(t)}{dt} = \frac{1}{L_r}V_{in} - \frac{v_c(t)}{L_r} - \frac{n}{L_r}\text{sign}(i_{Lr}(t) - i_{Lm}(t))v_o(t) \tag{2.3}$$

$$\frac{dv_c(t)}{dt} = \frac{i_{Lr}(t)}{C_r} \tag{2.4}$$

$$\frac{di_{Lm}(t)}{dt} = \frac{n}{L_m}v_o\text{sign}(i_{Lr}(t) - i_{Lm}(t)) \tag{2.5}$$

$$\frac{dv_o(t)}{dt} = \frac{n}{C_o}|i_{Lr}(t) - i_{Lm}(t)| - \frac{v_o(t)}{R_L}. \tag{2.6}$$

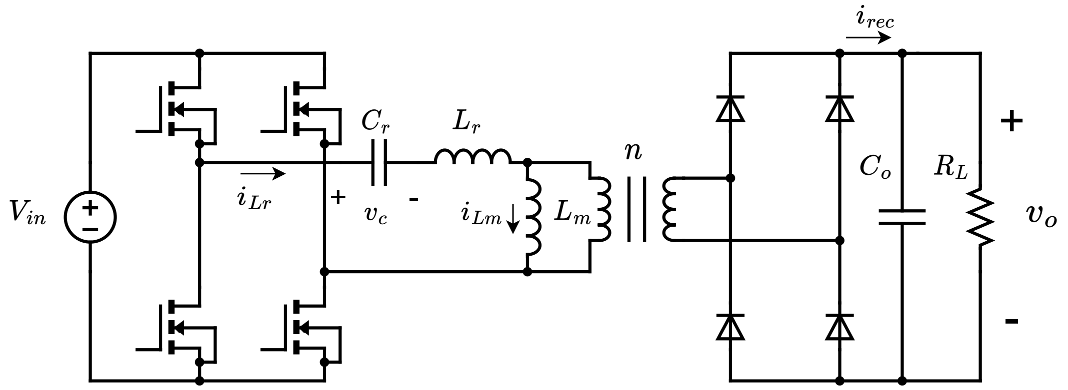

Figure 2.4: Full circuit diagram of the LLC converter.

As observed from (2.3)-(2.6), deriving a linearized model is a nontrivial task, due to the hard nonlinearities in the form of absolute value and signum functions. Moreover, since some state variables are sinusoidal quantities, determining a steady-state operating condition can also be difficult.

2.2.1 Extended Describing Function Method

The describing function method is a technique used to analyze the frequency response of nonlinear systems. As described in [7], a describing function of a nonlinearity ψ is obtained by applying a sinusoidal signal with amplitude a at the input and calculating the Fourier coefficient of the first harmonic at the output. The describing function is then simply the ratio between the Fourier coefficient and input amplitude a. Thus, the nonlinearity is approximated with an equivalent gain for a given frequency.

Describing functions have certain limitations, as mentioned in [8]. One of these limitations is that the nonlinearities they describe must be time-invariant. Another limitation is that their accuracy decreases significantly when applied to signals with multiple harmonics, as the approximation only considers the first harmonic. These limitations do not pose an issue for the resonant converter. The absolute value and signum functions are time-invariant. The resonant nature of the tank filters out most harmonics generated. Thus, the describing function method is a suitable approach for modeling the converter.

As explained in [6], a variant of the describing function called the extended describing function (EDF) can be applied to obtain a linear model of the converter. Firstly, the AC states are decomposed into a combination of sine and cosine terms.

$$i_{Lr}(t) = i_{rs}(t)\sin(\omega_s t) - i_{rc}(t)\cos(\omega_s t) \tag{2.7}$$

$$v_c(t) = v_{cs}(t)\sin(\omega_s t) - v_{cc}(t)\cos(\omega_s t) \tag{2.8}$$

$$i_{Lm}(t) = i_{ms}(t)\sin(\omega_s t) - i_{mc}(t)\cos(\omega_s t) \tag{2.9}$$

Then, the nonlinear terms are approximated by their describing functions to obtain the following equations.

$$L_r \frac{di_{rs}}{dt} = \frac{4V_{in}}{\pi} - L_r\omega_s i_{rs} - v_{cs} - \frac{4n}{\pi}\frac{(i_{rs} - i_{ms})}{i_p}V_o \tag{2.10}$$

$$L_r \frac{di_{rc}}{dt} = L_r\omega_s i_{rc} - v_{cc} - \frac{4n}{\pi}\frac{(i_{rc} - i_{mc})}{i_p}V_o \tag{2.11}$$

$$C_r \frac{dv_{cs}}{dt} = -C_r\omega_s v_{cc} + i_{rs} \tag{2.12}$$

$$C_r \frac{dv_{cc}}{dt} = C_r\omega_s v_{cs} + i_{rc} \tag{2.13}$$

$$L_m \frac{di_{ms}}{dt} = -L_m\omega_s i_{mc} + \frac{4n}{\pi}\frac{(i_{rs} - i_{ms})}{i_p}V_o \tag{2.14}$$

$$L_m \frac{di_{mc}}{dt} = L_m\omega_s i_{ms} + \frac{4n}{\pi}\frac{(i_{rc} - i_{mc})}{i_p}V_o \tag{2.15}$$

$$C_o \frac{dV_o}{dt} = \frac{2n}{\pi}i_p - \frac{n}{R_L}v_o \tag{2.16}$$

$$i_p = \sqrt{(i_{rs} - i_{ms})^2 - (i_{rc} - i_{mc})^2} \tag{2.17}$$

The nonlinearities have now been approximated by describing functions and the state equations in (2.10) can be linearized to obtain a state-space model. Due to the FHA assumption and the use of describing functions, the accuracy of the EDF model is slightly worse away from resonance.

2.2.2 Averaged Model

Another approach for modeling the LLC converter is to consider a simplified averaged circuit model [1]. This method approximates the voltage gain of the tank with a controlled voltage source. The average dynamic behavior is approximated using equivalent circuit elements. As mentioned in [1], the dynamic small-signal gain of the controlled voltage source can be derived using the derivative of the voltage gain from (2.3).

$$k_f = \frac{\partial K}{\partial F} \cdot \frac{V_{in}}{n} \cdot \frac{1}{f_r} \tag{2.18}$$

Through analysis of the switching cycles during resonant operation as shown in [1], the equivalent averaged circuit elements describing the tank dynamics at resonance (inductive region) can be derived as an equivalent series inductor L_{eq}.

$$L_{eq} = \frac{\pi^2}{4n^2} L_r \tag{2.19}$$

The resulting averaged model circuit is shown in Fig 2.5.

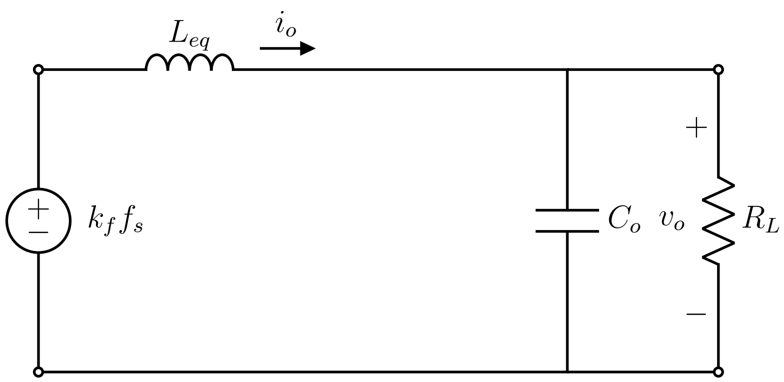

Figure 2.5: Average model equivalent circuit.

The averaged model circuit describes the converter through its averaged output quantities as shown in Fig 2.6. Therefore, unlike the previous models, this model does not include any AC state variables. However, this also results in lower accuracy as the high-frequency dynamics are neglected [1].

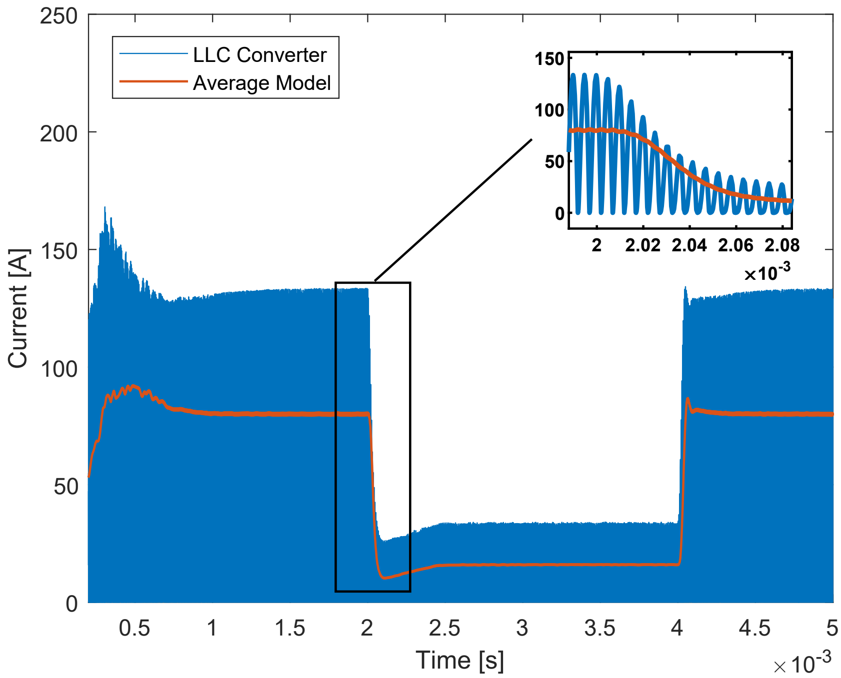

Figure 2.6: Output current from the average model.

From the average model circuit, the state equations can be derived using simple circuit analysis.

$$\begin{aligned} \frac{d}{dt}v_o &= \frac{-1}{C_o R_L}v_o + \frac{1}{C_o}i_o \\ \frac{d}{dt}i_o &= \frac{-1}{L_{eq}}v_o + \frac{k_f}{L_{eq}}f_s \end{aligned} \tag{2.20}$$

2.2.3 Model overview

A short overview of the models is shown in Table 2.1.

Table 2.1: Model overview.

	Nonlinear	**EDF**	**Average**
Model Order	4	7	2
Linear representation	No	Yes	Yes
AC State Variables	3	6	0
Accuracy	High	High-Medium	Medium-Low

The accuracy of the nonlinear model is the highest as it directly models the converter without any approximations, but it lacks a linear representation. The EDF model has slightly lower model accuracy due to the FHA and describing function approximations. However, the EDF method also results in an inflated model order with many AC state variables. The average model has a low model order with no AC state variables. However, due to the simplified circuit representation, the accuracy is lower compared to the EDF and nonlinear model.

2.3 Control Theory

The following section provides the theoretical foundation for the control methods used for the project. Firstly, the classical Proportional-Integral-Derivative (PID) is explained, followed by gain scheduling. Then, the corresponding robust model-based MIMO approaches are covered.

2.3.1 Classical PID Control

Classical control methods mainly rely on different variants of the PID controller, which is widely used due to its simple structure and implementation. The PID controller controls a system by continuously adjusting its own output based on the error $e(t)$ between the desired reference and the measured output [9]. This is achieved through three gain terms based on the error signal: the proportional, integral, and derivative terms as shown in (2.21).

$$u(t) = K_p \cdot e(t) + K_i \cdot \int e(\tau)d\tau + K_d \cdot \frac{d}{dt}e(t) \tag{2.21}$$

The proportional term relates to the magnitude of the error signal, while the integral term accumulates the error over time and reduces stationary errors [9]. The derivative term accounts for the rate of change of the error signal. In many practical applications, the derivative term is often omitted due to its sensitivity to measurement noise, resulting in a Proportional-Integral (PI) controller. Despite its simple structure and implementation, the PID controller has its limitations. One significant limitation is that it cannot handle MIMO systems without the use of inner and outer loops [10]. This additional complexity for MIMO systems can make controller tuning difficult, particularly for complex and nonlinear systems.

2.3.2 Gain scheduling

Gain scheduling is a concept in controller design, where the controller gains vary with respect to one or several scheduling parameters [10]. The idea of gain scheduling is to include the nonlinear dynamics in the controller design by switching through several linear controllers. Each controller is typically tuned for a specific operating point, and the corresponding gains are stored in a lookup table. The controller gains are then interpolated between the operating points.

Although gain scheduling can be effective in handling nonlinear dynamics, it has certain limitations. Specifically, the stability and performance of the controller can only be guaranteed at the exact tuning points, as the interpolation may not accurately describe the system dynamics between the operating points. Additionally, the implementation of a gain scheduled controller may require the scheduling parameters to be measured.

2.3.3 Robust Control

When dealing with nonlinear dynamics, an alternative approach is to design a robust controller that can handle a wide range of operating conditions. However, using this method can result in overly conservative controllers. The most commonly used framework for designing robust controllers is the $\mathcal{H}_2/\mathcal{H}_\infty$ framework. In this approach, the objective is to minimize the effect of disturbances d on the performance outputs z [10]. The design objectives are specified by arranging the plant model P into a generalized plant structure as shown in Fig 2.7. The aim is to find a controller K that takes input y and computes an output u such that the performance constraints on the performance outputs z are satisfied. The optimal controller is then found by minimizing the $\mathcal{H}_2/\mathcal{H}_\infty$ norm of the gain from d to z ($\min ||T_{zd}(s)||_{2/\infty}$). Additionally, the performance outputs can be weighted with transfer functions to provide more flexibility in tuning the controller.

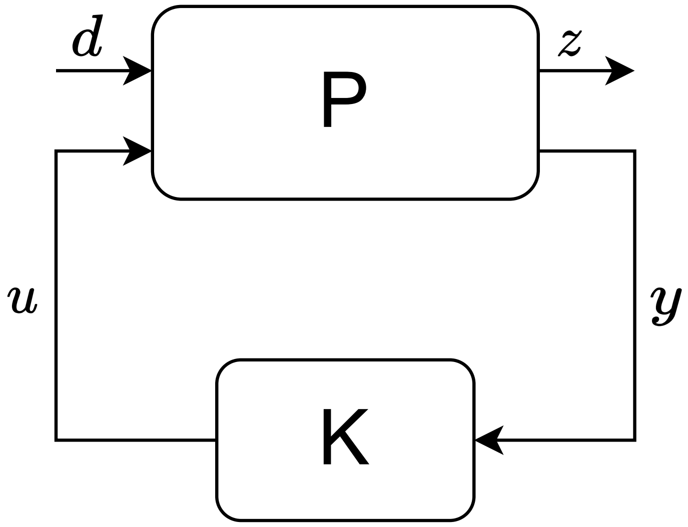

Figure 2.7: Generalized plant structure.

2.3.4 Linear parameter-varying control (LPV)

Another approach for handling the time-varying dynamics of a nonlinear plant is through the LPV framework. The time-varying nature of the plant is expressed as an affine parameter variation scheduled by $\rho(t)$ as shown in (2.22).

$$\begin{aligned} \dot{x}(t) &= A(\rho(t))x(t) + B(\rho(t))u(t) \\ y(t) &= C(\rho(t))x(t) + D(\rho(t))u(t) \end{aligned} \tag{2.22}$$

The LPV framework offers a potential solution to some of the limitations associated with gain scheduling. Specifically, it provides a more systematic approach to optimal control design. The LPVTools toolbox offers a range of tools and functions for the design of LPV models and controllers, as documented in [11]. Once an LPV model has been constructed, design objectives can be specified in the same way as for the robust control framework. The toolbox then finds a stable controller over the whole specified range of ρ while simultaneously minimizing the induced $\mathcal{L}_2$ norm [11] (i.e a scheduled $\mathcal{H}_\infty$ norm). Like the gain scheduled controller, the implementation of LPV controllers may also require the scheduling parameters to be measured.

3

Methods

The following chapter covers the methodology for achieving the previously stated objectives in Section 1. For analysis and testing of the models and control algorithms, the following component parameters were used for the LLC converter. These values were calculated from [2] for a 650 V to 24 V, 1920 kW converter with a resonance frequency of 100 kHz.

Table 3.1: LLC Parameters.

Parameter	**Value**
V_{in}	650 V
V_o	24 V
L_r	109 µH
C_r	23 nF
L_m	577 µH
f_r	100 kHz
P_o	1920 W
n	27.08
C_o	1 mF

3.1 Modeling

In this section, the different models were evaluated with regard to accuracy and suitability for control design. A new modified average model was also derived for the scheduled controller design.

3.1.1 Nonlinear model

A nonlinear model using the original state equations in (2.3) was implemented in Simulink for comparison with the linear models described in Section 2. The nonlinear model was verified by comparing it against an LLC converter built in Simscape Electrical. The nonlinear model is shown in Fig 3.1.

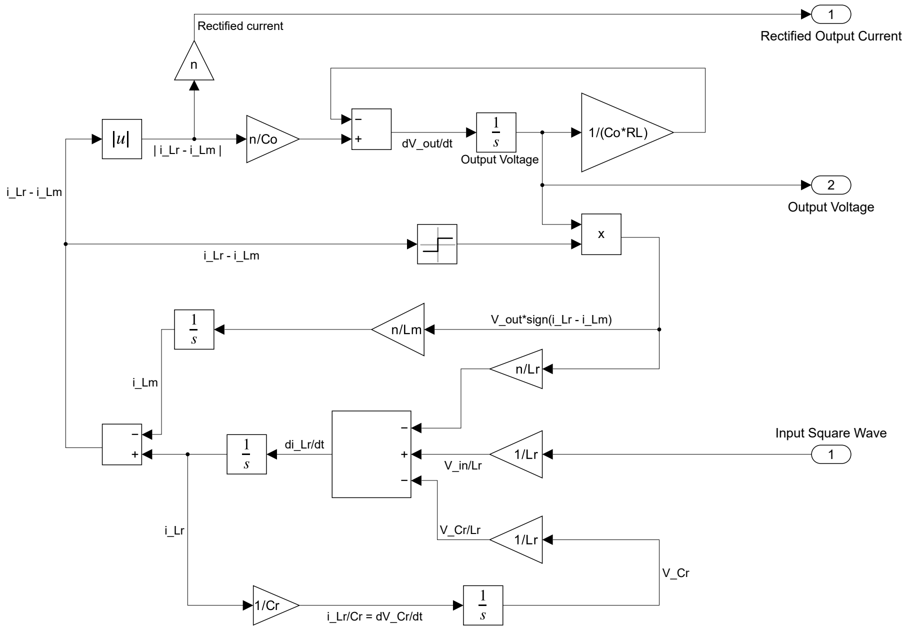

Figure 3.1: Nonlinear model in Simulink.

Initial tests with step responses for the nonlinear model at different switching frequencies are shown in Fig 3.2.

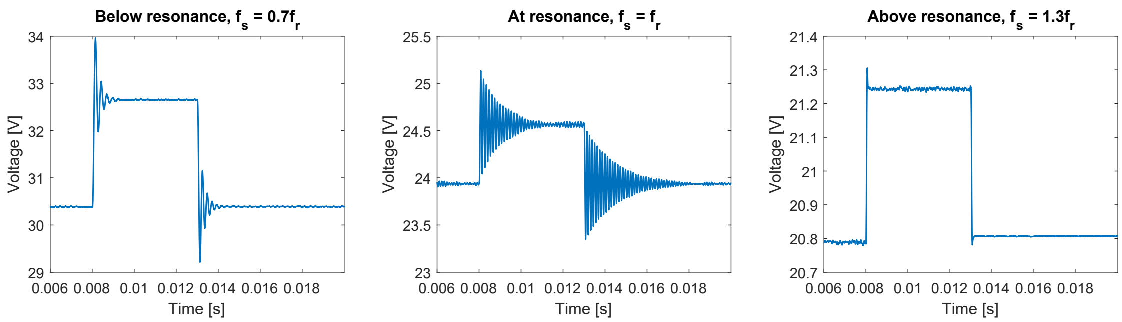

Figure 3.2: Step responses from the nonlinear model.

As expected, the converter displays different dynamics based on its operating point. The different operating modes mentioned in [2] result in varying dynamics for the converter. Thus, it is important that the model used for the control design describes this nonlinear behavior in some capacity.

3.1.2 Model analysis

In this section, the analytical properties of the existing models are investigated. Model accuracy and suitability for control design are also discussed.

3.1.2.1 EDF Model

The equations obtained from the EDF method can now be linearized using the conventional method with the Jacobian. The steady-state point $(\bar{x}, \bar{u})$ is found by defining an operating point (ω_s, R_L) and setting the time derivatives in (2.10) to zero. The state-space matrices A, B for the linearized model are then simply given by (3.2).

$$x = \begin{bmatrix} i_{rs} \\ i_{rc} \\ v_{cs} \\ v_{cc} \\ i_{ms} \\ i_{mc} \\ v_o \end{bmatrix} \qquad u = \omega_s \tag{3.1}$$

$$\begin{aligned} A_{ij} &= \left. \frac{\partial f(x(t), u(t))}{\partial f_j(t)} \right|_{\bar{x},\bar{u}} \\ B_{ij} &= \left. \frac{\partial f(x(t), u(t))}{\partial u_j(t)} \right|_{\bar{x},\bar{u}} \end{aligned} \tag{3.2}$$

The EDF model is a linearized model obtained by applying the EDF method to the original nonlinear equations. Thus, the EDF model should accurately portray the nonlinear one for a given operating point. A simulation of the step responses against the nonlinear model is shown in Fig 3.3.

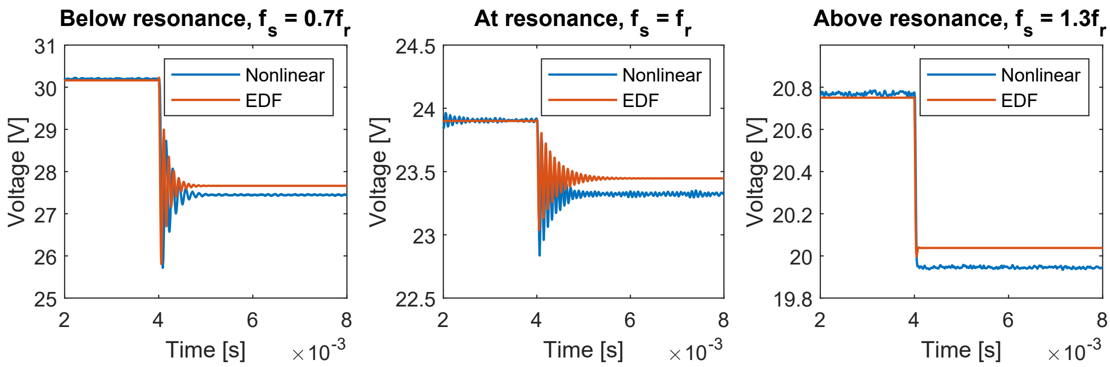

Figure 3.3: Step response comparison of EDF and nonlinear model.

There is a slight steady-state error due to the FHA approximation, but the dynamics for different operating points are similar. Although the dynamics match, the EDF model can be difficult to use for designing control algorithms. Analysis of the system controllability and observability using Kalman's test show that the system is neither controllable nor observable [3]. Therefore, in order to apply state feedback methods, the system must first be transformed into a minimal realization with a Kalman decomposition [12]. Another drawback is the use of sine-cosine decomposition for the original states. These decomposed states are not directly related to outputs from the actual system. This can complicate practical implementation as these states cannot be directly measured, leading to higher design complexity. Nonetheless, the EDF model still provides an accurate linearized model at a given operating point. Linear analysis tools can be applied to the model for validation of simplified models.

3.1.2.2 Average Model

From the state equations in (2.20), the linearized state-space representation can be derived.

$$\Delta \dot{x} = \begin{bmatrix} \Delta \dot{v_o} \\ \Delta \dot{i_o} \end{bmatrix} = \begin{bmatrix} \frac{-1}{C_o R_L} & \frac{1}{C_o} \\ \frac{-1}{L_{eq}} & 0 \end{bmatrix} \begin{bmatrix} \Delta v_o \\ \Delta i_o \end{bmatrix} + \begin{bmatrix} 0 \\ \frac{K_f}{L_{eq}} \end{bmatrix} \Delta f_s \tag{3.3}$$

The structure of the average model is more suited for implementing control algorithms due to its clear input and output relations. The output voltage and current from the converter are direct state variables of the model. Furthermore, the averaged behavior of the model means that no AC state variables need to be considered. However, linearizing the model at different operating points and simulating its step response shows that the dynamics are only accurate for one operating point (at resonance). Compared with the EDF model, the accuracy of the model is lower, as it only describes the dynamics at resonance. This can be confirmed by looking at the Bode plots in Fig 3.4. The frequency-dependent damping behavior is not present in the average model.

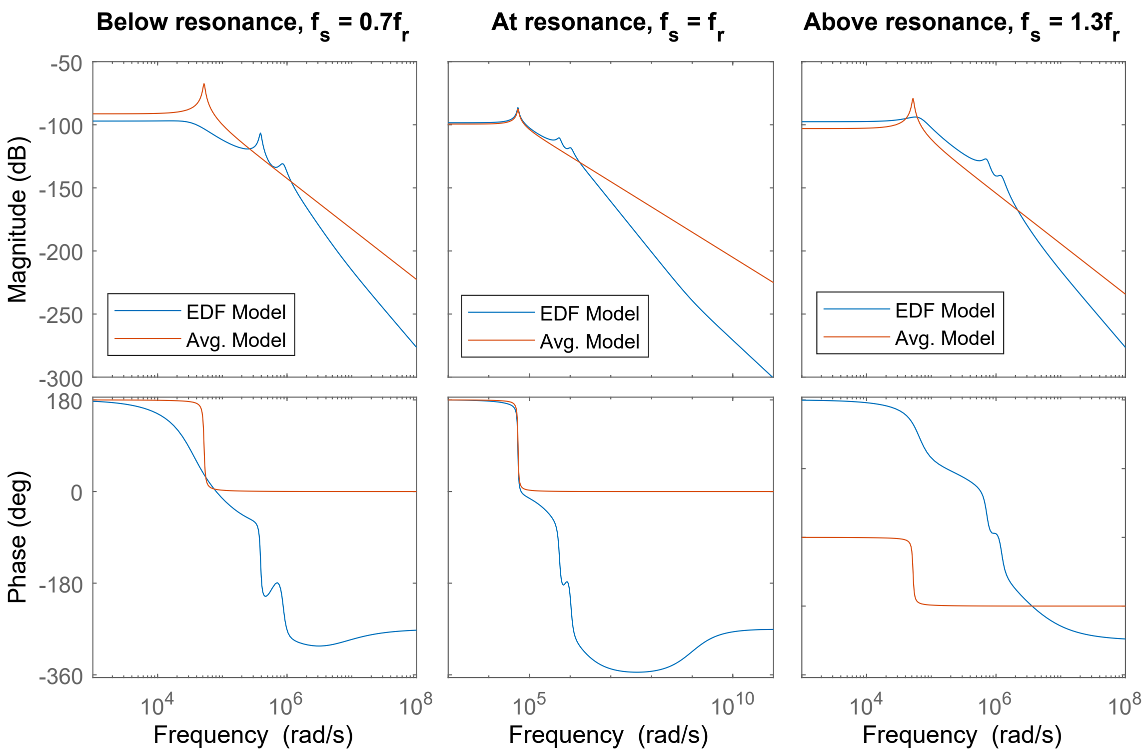

Figure 3.4: Control-to-Output Bode plots for Avg. model and EDF model.

3.1.3 Modified Average Model

In order to effectively use the average model to design a gain scheduled controller or an LPV controller, the average model has to be modified to include the frequency-dependent damping behavior. This frequency-dependent damping can be calculated from the poles of the EDF model. The EDF model is linearized at different frequencies and the damping ratio of the dominant pole pair (p, p^*) is calculated according to (3.4) and plotted in Fig 3.5.

$$\zeta = -cos(\angle p) \tag{3.4}$$

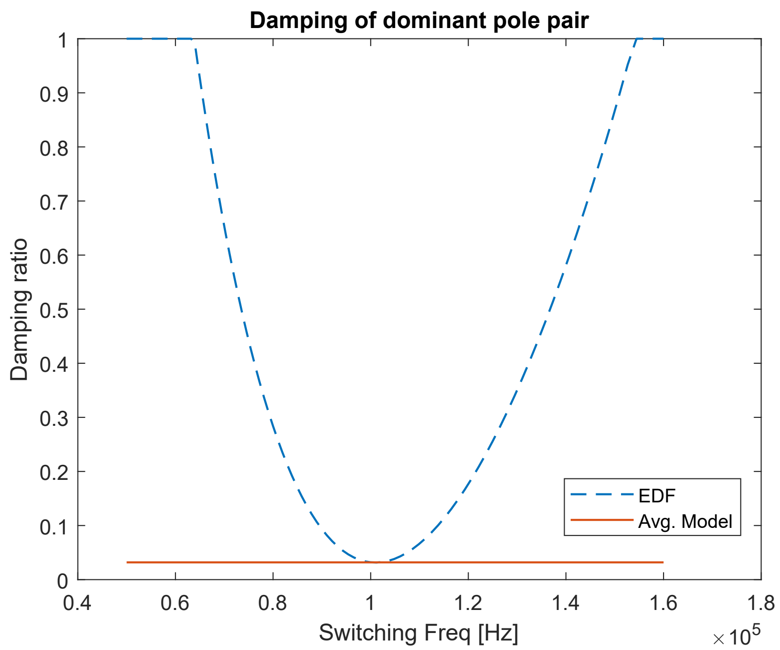

Figure 3.5: Damping ratio for Avg. model and EDF model.

As observed, the damping is lowest at resonance and increases as the system moves away from resonance. Clearly, the equivalent series inductor L_{eq} is not sufficient to model the change in the damping due to switching frequency. Additional damping elements have to be added to obtain the correct damping behavior. As explained in [13], [14], the damping of the converter is related to the resonant tank impedance. In order to model this behavior, a frequency-varying resistor R_s can be added in series with L_{eq} as shown in Fig 3.6.

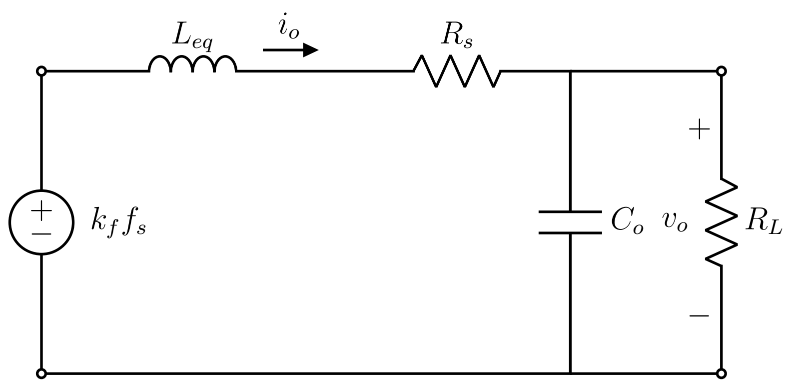

Figure 3.6: Modified Average model circuit.

As discussed in [13], [14], the resistor R_s functions as a frequency-varying damping term to modify the damping of the circuit according to (3.5).

$$R_s = \frac{L_{eq}(\omega_s L_r - \frac{1}{\omega_s C_r})(\omega_s - \omega_r)}{R_{ac}} \tag{3.5}$$

Furthermore, L_{eq} also needs to be frequency-varying according to (3.6) in order to correctly model the beat frequency [13], [14].

$$L_{\text{eq}} = \begin{cases} \frac{\pi^2}{8}\frac{L_r}{n^2}\left[1 + \frac{f_r^2}{f_\text{s}^2} + \frac{L_m}{L_r}\left(1 - \frac{f_\text{s}}{f_r}\right)\right] & f_\text{s} < f_r \\ \frac{\pi^2}{4}\frac{L_r}{n^2}, & f_\text{s} = f_r \\ \frac{\pi^2}{8}\frac{L_r}{n^2}\left(1 + \frac{f_r^2}{f_\text{s}^2}\right) & f_\text{s} > f_r \end{cases} \tag{3.6}$$

After this modification, the damping ratio for both models was calculated and plotted again in Fig. 3.7.

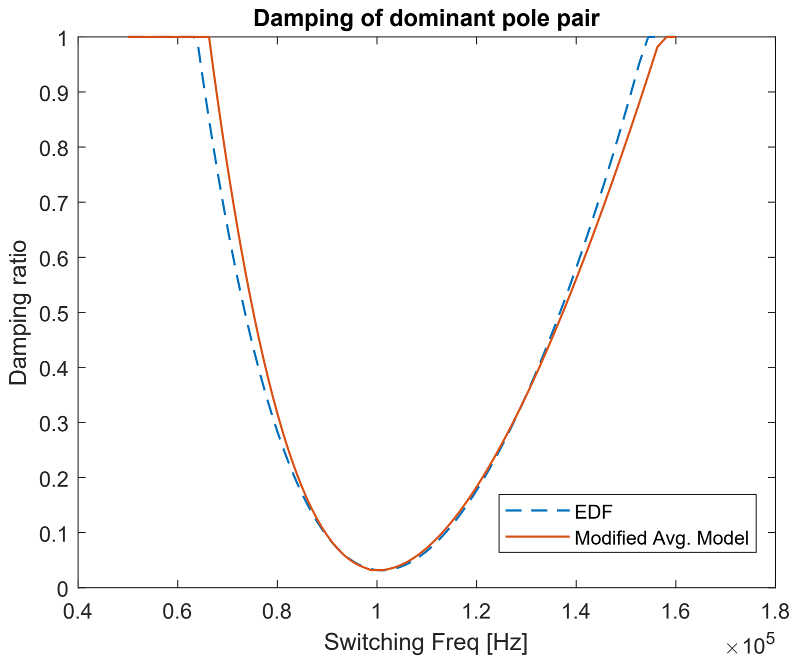

Figure 3.7: Damping ratio for Modified Avg. model and EDF model.

It can be observed that the damping of the modified average model corresponds to that of the EDF model. The magnitude and phase plots are also shown in Fig 3.8. It should be noted that the phase plots for $f_s = 1.3f_r$ may appear mismatched due to a lack of phase wrapping. However, upon closer examination, it is evident that the phase plots align but are merely shifted by 360°.

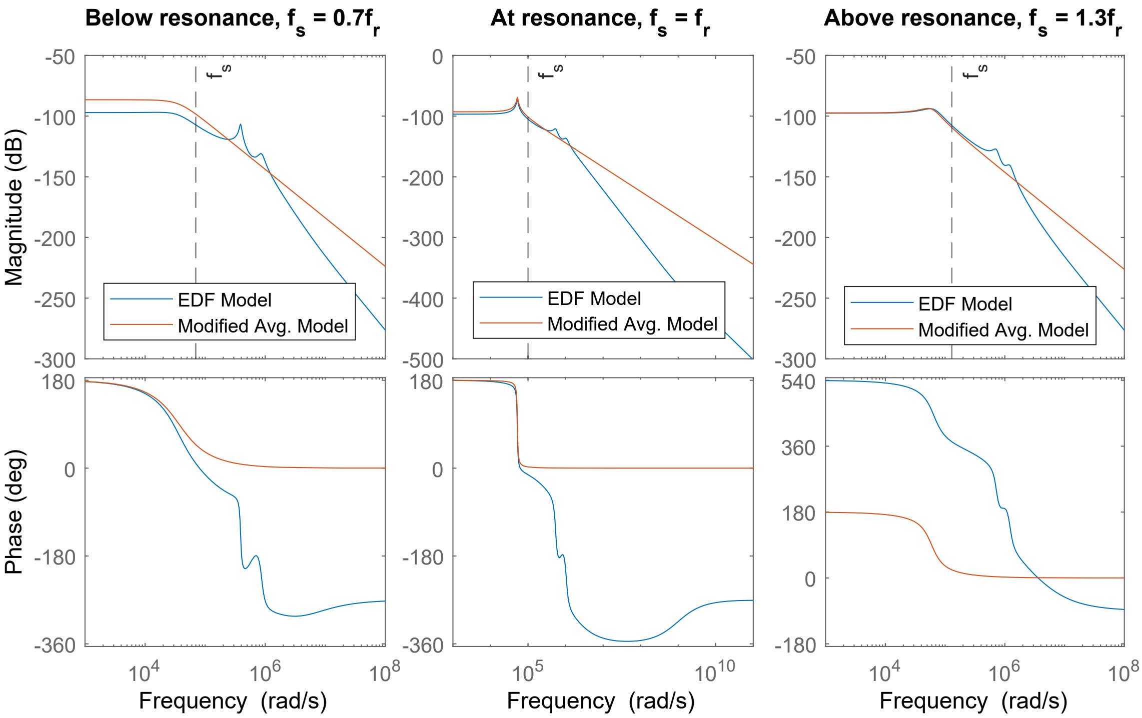

Figure 3.8: Control-to-Output Bode plots for Mod. Avg. model and EDF model.

The magnitude and phase plots match up to the switching frequency f_s, which is sufficient for the control design of LLC converters as explained in [15]. The modified model in (3.7) can be then derived through the modified circuit in Fig 3.6 along withy (3.5)-(3.6). This modified average model now contains the frequency-dependent damping behavior of the EDF model along with a simpler model structure that is suitable for the implementation of control algorithms.

$$\Delta\dot{x} = \begin{bmatrix} \Delta\dot{v}_o \\ \Delta\dot{i}_o \end{bmatrix} = \begin{bmatrix} \frac{-1}{CoR_L(t)} & \frac{1}{C_o} \\ \frac{-1}{L_{eq}(f_s(t))} & \frac{R_s(f_s(t),R_L(t))}{L_{eq}(f_s(t))} \end{bmatrix} \begin{bmatrix} \Delta v_o \\ \Delta i_o \end{bmatrix} + \begin{bmatrix} 0 \\ \frac{K_f(f_s(t),R_L(t))}{L_{eq}(f_s(t))} \end{bmatrix} \Delta f_s \tag{3.7}$$

Now the plant can also be implemented as an LPV model. More specifically, a quasi-LPV model as the scheduling parameters are part of the states and inputs. A requirement of an LPV model is state consistency [11], meaning that the state vector must remain consistent for all values of the scheduling parameters. The ordering and interpretation of state vector should remain the same, irrespective of the value of the scheduling parameters. This is not the case for (3.7) as the state and input vectors are defined as offsets from a linearizing point $(x - \bar{x},\, u - \bar{u})$. Therefore, a small modification is needed to ensure state consistency for (3.7) by parameterizing the offset from the linearization point as shown in (3.8).

$$
\begin{aligned}
\Delta\dot{x}(\rho) &= A(\rho)\Delta x(\rho) + B(\rho)\Delta u(\rho) \Rightarrow \\
\dot{x} - \dot{\bar{x}} &= A(\rho)(x - \bar{x}(\rho)) + B(\rho)(u - \bar{u}(\rho)) \Rightarrow \\
\dot{x} &= A(\rho)x + B(\rho)u - \underbrace{(A(\rho)\bar{x}(\rho) + B(\rho)\bar{u}(\rho))}_{\bar{E}(\rho)} \Rightarrow \\
\dot{x} &= A(\rho)x + \begin{bmatrix} B(\rho) & -\bar{E}(\rho) \end{bmatrix} \begin{bmatrix} u \\ 1 \end{bmatrix} \\
\rho &= \begin{bmatrix} R_L(t) & f_s(t) \end{bmatrix}
\end{aligned}
\tag{3.8}
$$

A comparison between the nonlinear model and LPV model for different input steps is shown in Fig 3.9.

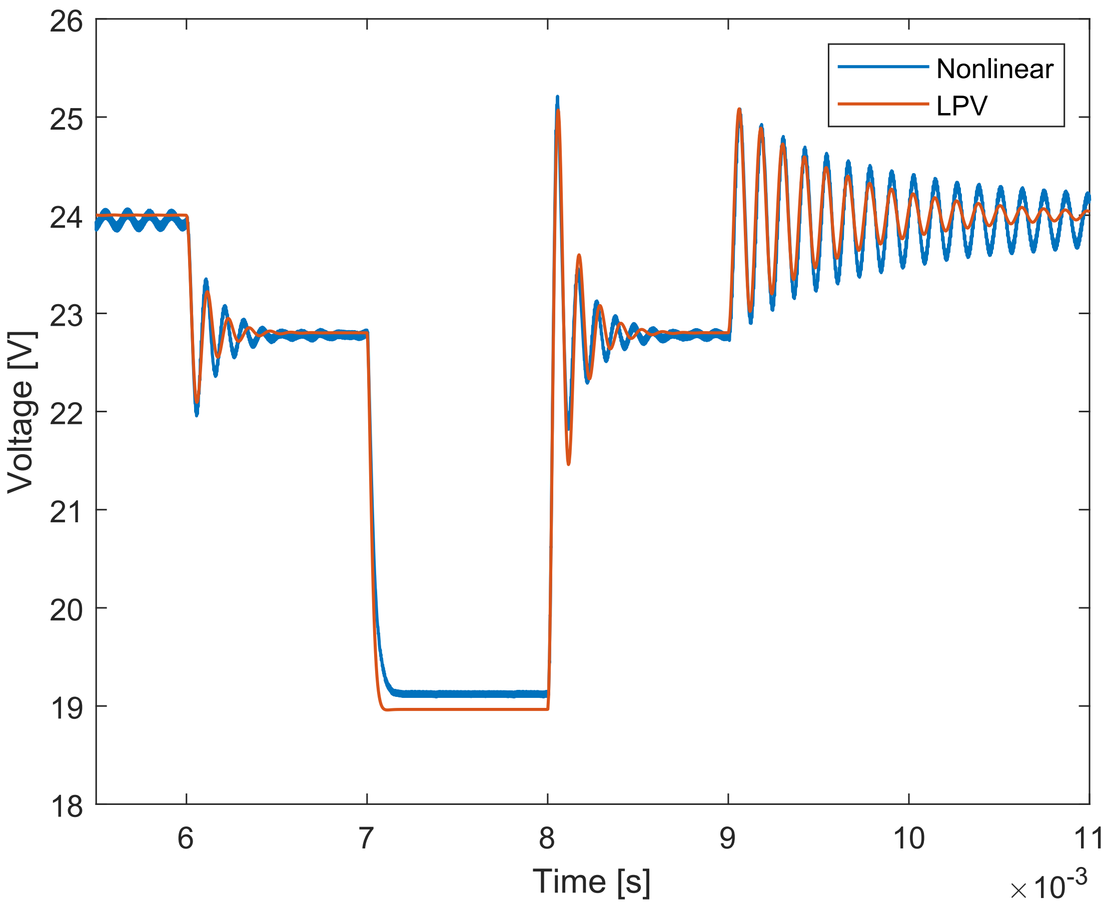

Figure 3.9: Step response comparison for nonlinear and LPV model.

3.2 Control design

This section presents the implementation of all controllers, including the specification of weights and parameters used for tuning the controllers.

3.2.1 Cascaded PI Controller

As highlighted in Section 2, conventional PI controllers are unable to handle MIMO systems unless inner and outer control loops are introduced. Thus, a cascaded PI controller is implemented to regulate both current and voltage. The control objective is to track a voltage reference while minimizing significant fluctuations in the output current. According to [1], this type of controller has shown promising performance when tuned using the average model.

The controller consists of an inner current loop tuned to 10 times the bandwidth of the outer voltage loop. This approach simplifies the controller tuning since the inner loop is much faster and can be regarded as constant. The idea of this approach is to reject load (current) disturbances before they can propagate to the rest of the system.

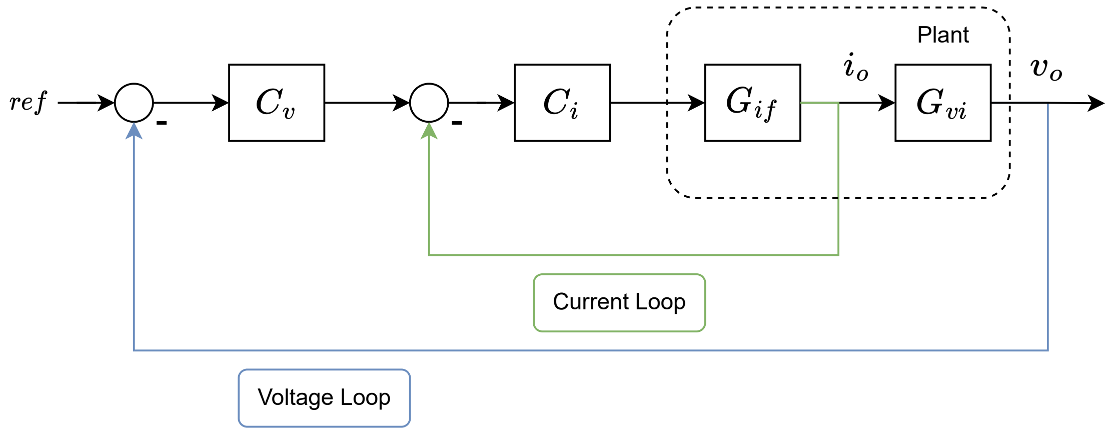

Figure 3.10: Cascaded PI Block Diagram.

Transfer functions describing the frequency-to-current $G_{if}(s)$ and current-to-voltage $G_{vi}(s)$ relations were derived from the average model in (2.20) in order to tune the controllers.

$$G_{if}(s) = k_f \frac{\frac{1}{R_L} + sC_o}{s^2 L_{eq} C_o + s\frac{sL_{eq}}{R_L} + 1} \tag{3.9}$$

$$G_{vi}(s) = \frac{1}{\frac{1}{R_L} + sC_o} \tag{3.10}$$

The linearizing point was selected at resonance ($F = 1$) with 50% load ($R_L = 0.6\ \Omega$) to reflect the average operating conditions. The controllers were tuned by specifying a desired bandwidth and phase margin with `pidtune()` in MATLAB. The tuning was performed according to [16]. First, the inner loop controller C_i is tuned for G_{if}. Then, the inner closed loop is formed as $G_{cl} = (G_{if}C_i)/(1 + G_{if}C_i)$. Finally, the outer loop controller C_v is tuned for $G_{cl}G_{vi}$. As recommended in [1], an inner loop bandwidth of 10 kHz and an outer loop bandwidth of 1 kHz with 60° phase margin was used.

3.2.2 Gain Scheduled Cascaded PI Controller

The gain scheduled PI controller was tuned similarly to the nominal case. The controllers were tuned for each operating point in the parameter grid as shown in Table 3.2. For each operating point, the corresponding transfer functions $G_{if}(f_s, R_L)$ and $G_{vi}(f_s, R_L)$ were calculated and used to compute the controller gains. The same bandwidths as in the nominal case were used. The controller gains were then stored in a lookup table to schedule the controller.

Table 3.2: Parameter grid for scheduled controllers.

Scheduling parameter	**Min**	**Max**	**No. points**
Switching Frequency f_s [kHz]	70	200	10
Output Load R_L [Ω]	0.3	3	10

3.2.3 $\mathcal{H}_\infty$ Controller

To design an optimal $\mathcal{H}_\infty$ controller, the operating point of the nominal plant G was selected to be the same as those for the nominal PI controller case, specifically at resonance and for 50% load. The generalized plant structure P was then constructed from G as shown below in Fig 3.11 with the weights and performance outputs described in Table 3.3. The $\mathcal{H}_\infty$ controller is then synthesized using `hinfsyn()` in MATLAB.

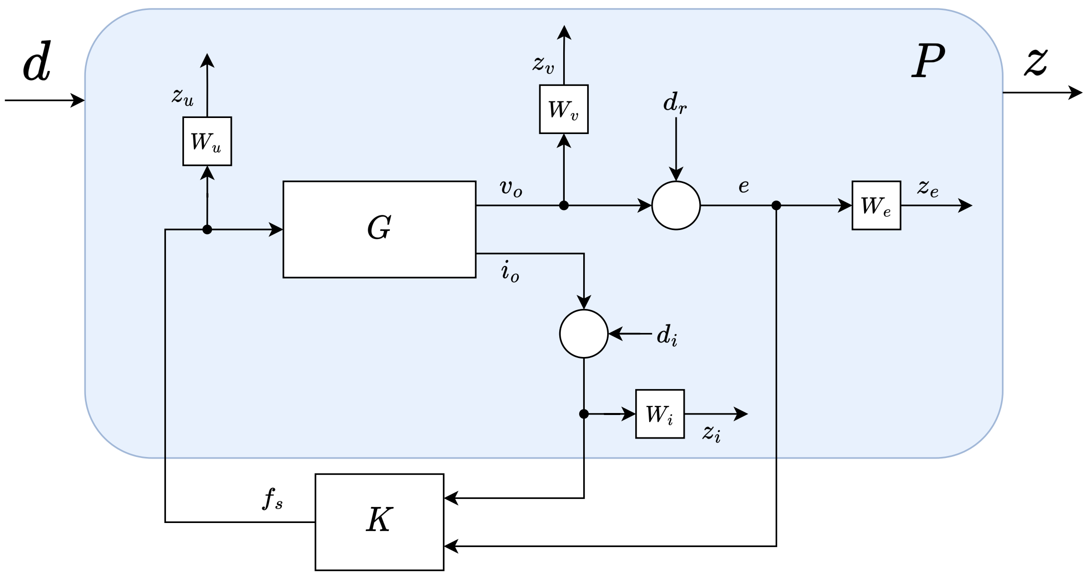

Figure 3.11: Generalized plant for $\mathcal{H}_\infty$ controller synthesis.

Table 3.3: Performance outputs and weights for $\mathcal{H}_\infty$.

Performance Outputs	**Weight**	**Transfer function**
Output Voltage, z_v	W_v	0.4
Output Current, z_i	W_i	0.1
Control Input, z_u	W_u	$\frac{s+2.17\cdot 10^5}{s+2.17\cdot 10^6}$
Output Voltage error, z_e	W_e	$\frac{0.0015s+989}{s+9.89}$

3.2.4 Uncertain $\mathcal{H}_\infty$ Controller

The design process for the uncertain $\mathcal{H}_\infty$ controller is similar to nominal $\mathcal{H}_\infty$ design. The modified average model is used to construct an uncertain state-space model (`uss`) in MATLAB. The model uncertainty was specified to be the same as the parameter grid used for the gain scheduled controller. The uncertain state-space model is augmented to a generalized plant P with weights according to Table 3.4. The uncertain $\mathcal{H}_\infty$ controller is then synthesized using `musyn()` in MATLAB (μ-synthesis).

Table 3.4: Performance outputs and weights for uncertain $\mathcal{H}_\infty$.

Performance Outputs	**Weight**	**Transfer function**
Output Voltage, z_v	W_v	0.4
Output Current, z_i	W_i	0.05
Control Input, z_u	W_u	$\frac{50s+2.65\cdot 10^5}{s+2.65\cdot 10^4}$
Output Voltage error, z_e	W_e	$\frac{s+1.9\cdot 10^4}{s+4}$

3.2.5 LPV Controller

The LPVTools toolbox allows straightforward synthesis of an LPV controller with the same robust control framework. A parameter-varying state-space model (`pss`) is constructed with LPVTools using the parameter grid in Table 3.5 and the state-space model in (3.8). The generalized plant P with weights described in Table 3.5 is then used to synthesize the controller with `lpvsyn()`.

Table 3.5: Performance outputs and weights for LPV.

Performance Outputs	**Weight**	**Transfer function**
Output Voltage, z_v	W_v	0.4
Output Current, z_i	W_i	0.005
Control Input, z_u	W_u	$\frac{s+1.09\cdot 10^5}{s+1.09\cdot 10^8}$
Output Voltage error, z_e	W_e	$\frac{0.0015s+989}{s+1.97}$

3.3 Evaluation

The controllers are simulated with the nonlinear model in Simulink for evaluation. The voltage and current outputs from the nonlinear model are low-pass filtered to obtain the averaged values needed for the controller. A second-order Butterworth filter with a cutoff frequency of 20 kHz is used for this. The scheduled controllers assume ideal measurement of the scheduling signals. The controllers are evaluated for two disturbance scenarios.

- Load regulation
- Line regulation

3.3.1 Load regulation

Load regulation refers to the capability to maintain a constant output voltage in the presence of abrupt changes in the output load [17]. As the load can vary drastically during the operation of the converter, load regulation is an important metric for assessing performance. From a control perspective, this can be viewed as output disturbance rejection. The load disturbance is simulated as an instant change in the R_L parameter for the nonlinear model.

3.3.2 Line regulation

Line regulation refers to the capability to maintain a constant output voltage despite fluctuations in the input voltage [17]. Although the input voltage may experience some variations during operation, compared to load changes these variations are typically much smaller and within specified limits. As a result, line regulation is not as critical as load regulation. In control terminology, this is the same as input disturbance rejection. The input disturbance is simulated as an instant change in the supply voltage V_{in} for the nonlinear model.

3.3.3 Operating conditions

Each test scenario is also evaluated for different operating conditions to see how each controller handles the nonlinear characteristics of the system.

- Below resonance
  - Much higher voltage gain
  - Slightly damped
- At resonance (nominal)
  - Nominal voltage gain
  - Underdamped
- Above resonance
  - Slightly lower voltage gain
  - Overdamped

Finally, the evaluation is repeated for a perturbed plant as well, where the actual plant parameters differ from the ones used for the control design. The perturbed plant is modeled with 50% inductance loss for the inductors and 10% capacitance loss for the capacitor, which represents a common scenario. As mentioned in [18], capacitor aging results in loss of capacitance. Inductors can also lose inductance due to saturation, as discussed in [19].

Table 3.6: Perturbed LLC tank Parameters.

Parameter	**Value**
L_{rp}	55 µH
C_{rp}	21 nF
L_{mp}	289 µH
C_{op}	0.9 mF

4

Results

This chapter presents the results obtained from evaluating the disturbance rejection capability of the different controllers. The performance of the controllers is evaluated through a load disturbance test, followed by an input disturbance test. The evaluation is done for both a nominal plant and a perturbed plant.

4.1 Disturbances

The disturbances are simulated as instantaneous changes in the plant parameters. For the load disturbance, the output load starts at 100% and is stepped down to 20% before returning to 100% after 5 ms. For the input disturbance, the input voltage starts at 650 V and is stepped to 550 V (15%) before returning to 650 V after 5 ms. The disturbance signals are shown in Fig 4.1.

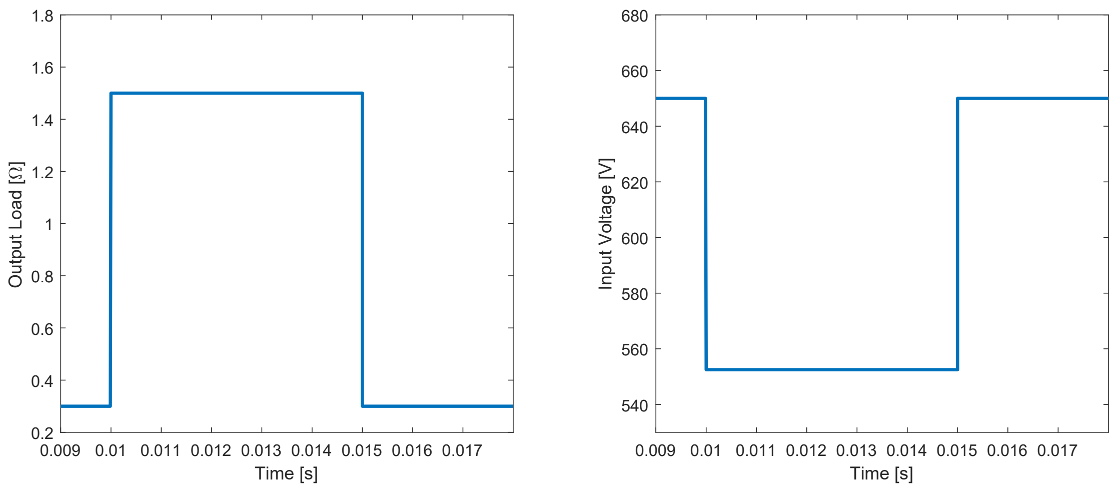

Figure 4.1: Load disturbance signals.

4.2 Nominal model

The disturbance rejection was tested for a nominal plant, meaning the same plant parameters in Table 3.1 were used for both the control design and the simulated model.

4.2.1 Load disturbance

The simulation results for the load disturbance test are shown in Fig 4.2. The PI controllers and robust controllers were plotted separately due to different scales in overshoot.

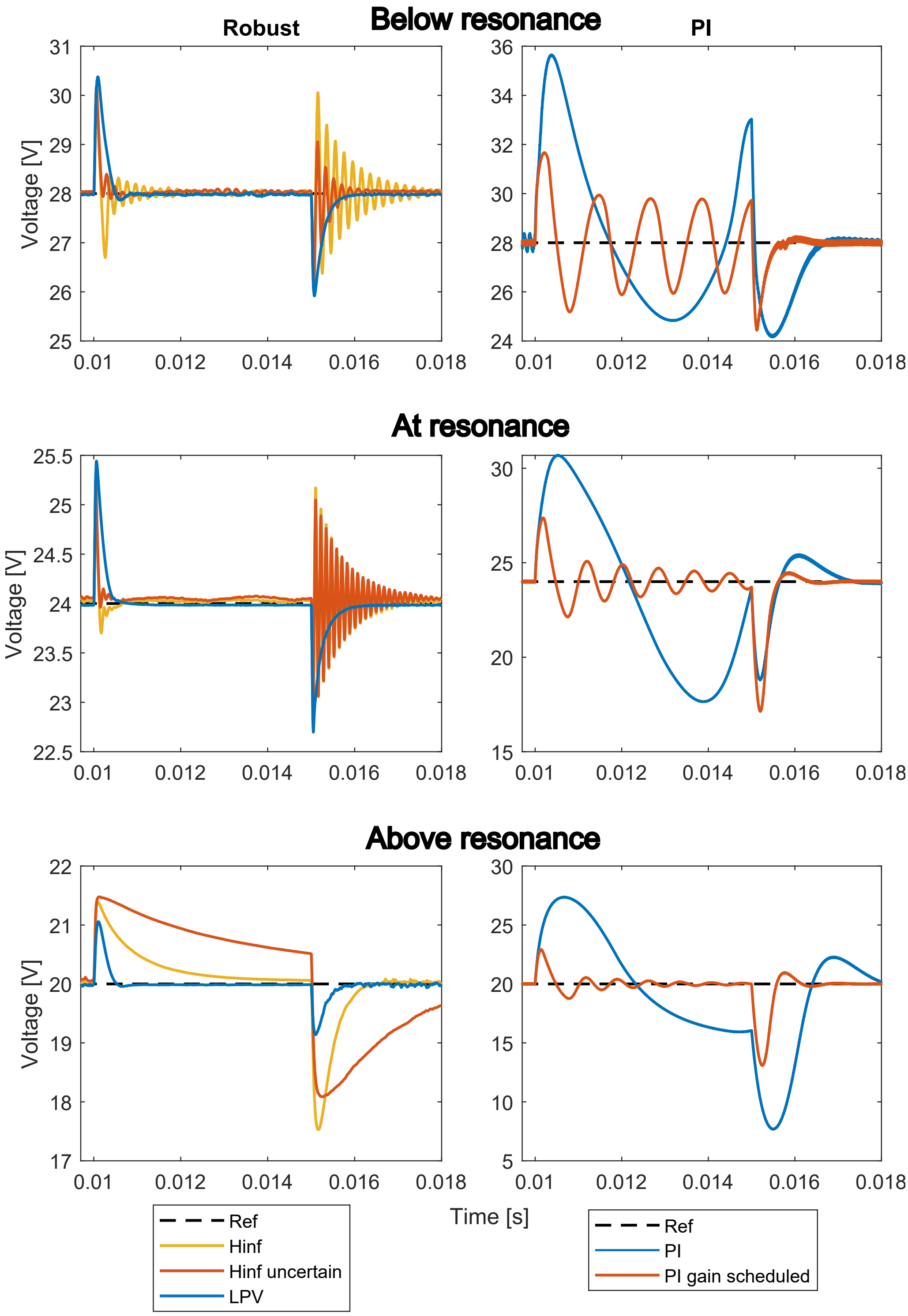

Figure 4.2: Load disturbance rejection for nominal plant.

The relative overshoot and transient recovery times were also calculated for easier comparison. The recovery time was defined as the time taken for the oscillation amplitude to settle within 1% of the nominal output voltage. These are shown in Tables 4.1-4.3. As the time between the disturbance steps was 5 ms, recovery times longer than 5 ms could not be calculated. Consequently, if the first step did not settle within 5 ms, metrics for the second step are omitted (-) since the step would have occurred during a transient.

Table 4.1: Overshoot and recovery times for load disturbance rejection below resonance for nominal plant.

Below resonance - 28 V	**PI**	**PI GS**	**Hinf**	**Hinf u**	**LPV**
Step 1 - Rel. overshoot	27.1%	13.1%	7.5%	7.5%	8.4%
Step 1 - Recovery time	-	-	1 ms	0.8 ms	0.6 ms
Step 2 - Rel. overshoot	-	-	7.4%	7.4%	7.5%
Step 2 - Recovery time	-	-	1.6 ms	0.7 ms	0.6 ms

For below resonance operation, the robust controllers showed significantly better performance compared to the PI controllers in terms of overshoot and settling time. All robust controllers settled within 2 ms and maintained overshoots below 10%. Among the robust controllers, the $\mathcal{H}_\infty$ controller was the slowest, showing large oscillations during the second step. The uncertain $\mathcal{H}_\infty$ controller was slightly better with less oscillatory behavior. Conversely, the LPV controller had the fastest recovery times without any oscillations but slightly larger overshoots. The PI controllers performed poorly with large overshoots and unstable behavior. However, it is worth noting that the gain scheduled controller did give a substantial improvement compared to the nominal case.

Table 4.2: Overshoot and recovery times for load disturbance rejection at resonance for nominal plant.

At resonance - 24 V	**PI**	**PI GS**	**Hinf**	**Hinf u**	**LPV**
Step 1 - Rel. overshoot	27.8%	13.7%	5.5%	5.5%	6%
Step 1 - Recovery time	-	-	0.3 ms	0.3 ms	0.3 ms
Step 2 - Rel. overshoot	-	-	4.6%	4.6%	5.5%
Step 2 - Recovery time	-	-	1.3 ms	1.3 ms	0.4 ms

For at resonance operation, the results were similar to the previous scenario, with the robust controller outperforming the PI controllers. The $\mathcal{H}_\infty$ and uncertain $\mathcal{H}_\infty$ continued to show the same oscillatory behavior for the second step. The LPV controller was again the fastest controller with no oscillations. The PI controllers performed slightly better at resonance compared to the previous case. Although the overshoots remained large and settling times were still long, the controllers do not appear to be unstable anymore.

Table 4.3: Overshoot and recovery times for load disturbance rejection above resonance for nominal plant.

Above resonance - 20 V	**PI**	**PI GS**	**Hinf**	**Hinf u**	**LPV**
Step 1 - Rel. overshoot	36.5%	14.5%	7.3%	7.4%	5%
Step 1 - Recovery time	-	3 ms	1.7 ms	-	0.4 ms
Step 2 - Rel. overshoot	-	39.5%	12.5%	-	5%
Step 2 - Recovery time	-	1.3 ms	1.5 ms	-	0.4 ms

For above resonance operation, the scheduled controllers perform much better than their counterparts. Both the gain scheduled PI and LPV controller recovered significantly faster with smaller overshoots. The $\mathcal{H}_\infty$ controller and uncertain $\mathcal{H}_\infty$ recovered much slower, especially the uncertain $\mathcal{H}_\infty$.

Overall, the nominal PI controller showed very poor performance. While the gain scheduled PI controller showed substantial improvement compared to the nominal case, it still performed poorly when compared to the robust controllers. The nominal $\mathcal{H}_\infty$ and uncertain $\mathcal{H}_\infty$ showed similar behavior with some differences above and below resonance. Specifically, the nominal $\mathcal{H}_\infty$ had a faster recovery above resonance, while the uncertain $\mathcal{H}_\infty$ had a faster recovery below resonance. The LPV controller performed the best across all operating conditions, with very consistent behavior.

4.2.2 Input disturbance

The simulation results for the input disturbance test are shown in Fig 4.3. The PI controllers and robust controllers were plotted separately due to different scales in overshoot.

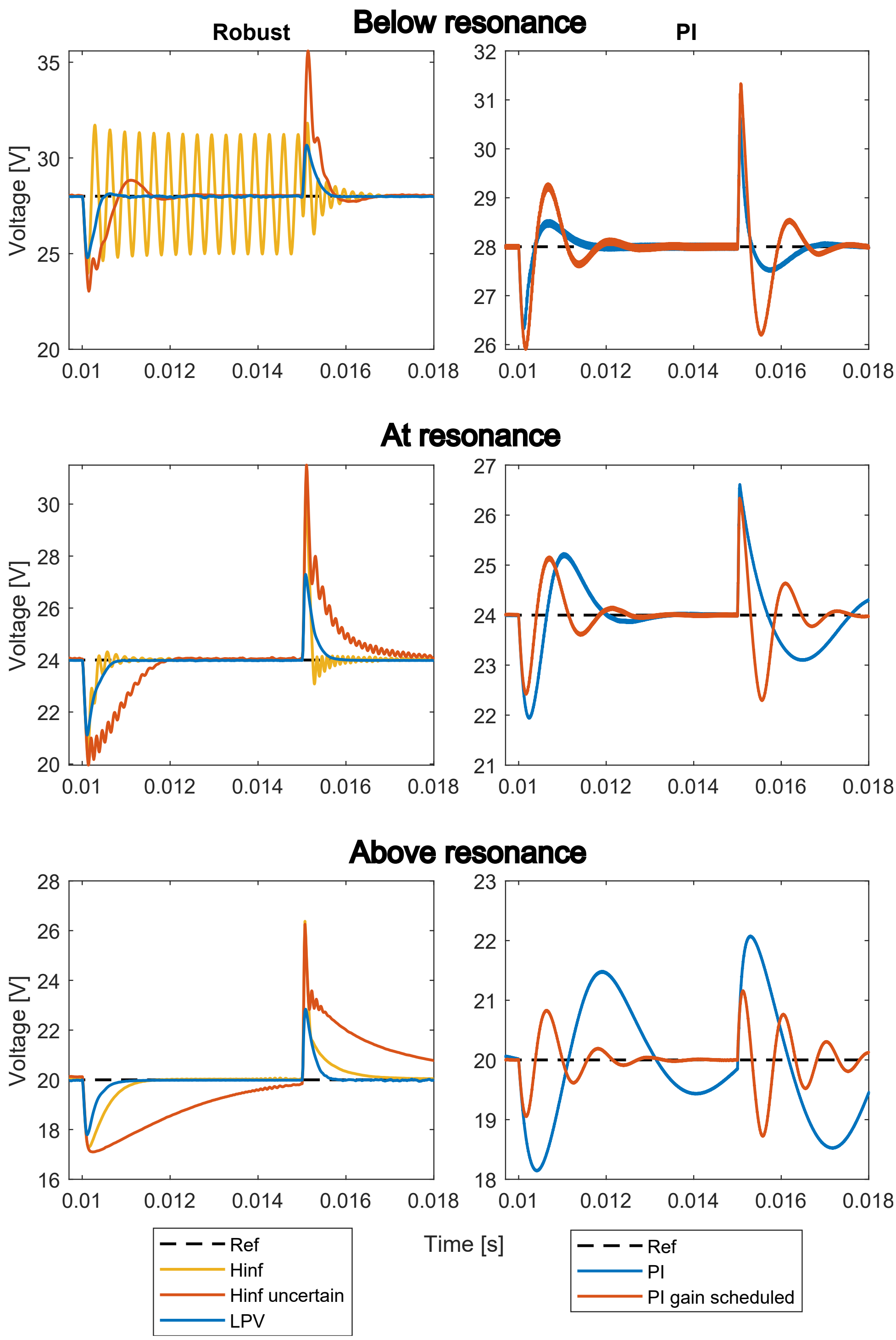

Figure 4.3: Input disturbance rejection for nominal plant.

Table 4.4: Overshoot and recovery times for input disturbance rejection below resonance for nominal plant.

Below resonance - 28 V	**PI**	**PI GS**	**Hinf**	**Hinf u**	**LPV**
Step 1 - Overshoot	5.5%	7.5%	14.3%	17.8%	11.7%
Step 1 - Recovery time	1.1 ms	1.7 ms	-	1.5 ms	0.4 ms
Step 2 - Overshoot	9.2%	11.7%	-	26.8%	9.4 %
Step 2 - Recovery time	1.3 ms	1.5 ms	-	0.7 ms	0.5 ms

Table 4.5: Overshoot and recovery times for input disturbance rejection at resonance for nominal plant.

At resonance - 24 V	**PI**	**PI GS**	**Hinf**	**Hinf u**	**LPV**
Step 1 - Overshoot	8.4%	6.6%	18.7%	18.7%	12%
Step 1 - Recovery time	1.8 ms	1.7 ms	0.6 ms	1.7 ms	0.6 ms
Step 2 - Overshoot	10.8%	10.7%	31.2%	31.2%	13.7%
Step 2 - Recovery time	-	1.8 ms	0.6 ms	2.3 ms	0.6 ms

Table 4.6: Overshoot and recovery times for input disturbance rejection above resonance for nominal plant.

Above resonance - 20 V	**PI**	**PI GS**	**Hinf**	**Hinf u**	**LPV**
Step 1 - Overshoot	9.3%	5%	13.5%	14.5%	11%
Step 1 - Recovery time	-	1.5 ms	1.1 ms	5 ms	0.6 ms
Step 2 - Overshoot	-	6%	29.3%	29.3%	14.2%
Step 2 - Recovery time	-	2.5 ms	1.3 ms	-	0.5 ms

For input disturbances, the performance of the robust controllers showcased similar trends as in the load disturbance case. The nominal $\mathcal{H}_\infty$ controller had a faster recovery above resonance, while the uncertain $\mathcal{H}_\infty$ controller was faster below resonance. Among the robust controllers, the LPV controller remained the superior choice, with the shortest recovery times and smallest overshoots.

In contrast, the PI controllers showcased better performance for input disturbances, with smaller overshoots compared to the robust controllers. The recovery times were also in the same range as those of the robust controllers. Unlike the load disturbance test, the gain scheduling did not give a substantial improvement compared to the nominal PI, except when operating above resonance.

4.3 Perturbed model

The perturbed model uses the component values in Table 3.6 for the simulated model and the values in Table 3.1 for control design.

4.3.1 Load disturbance

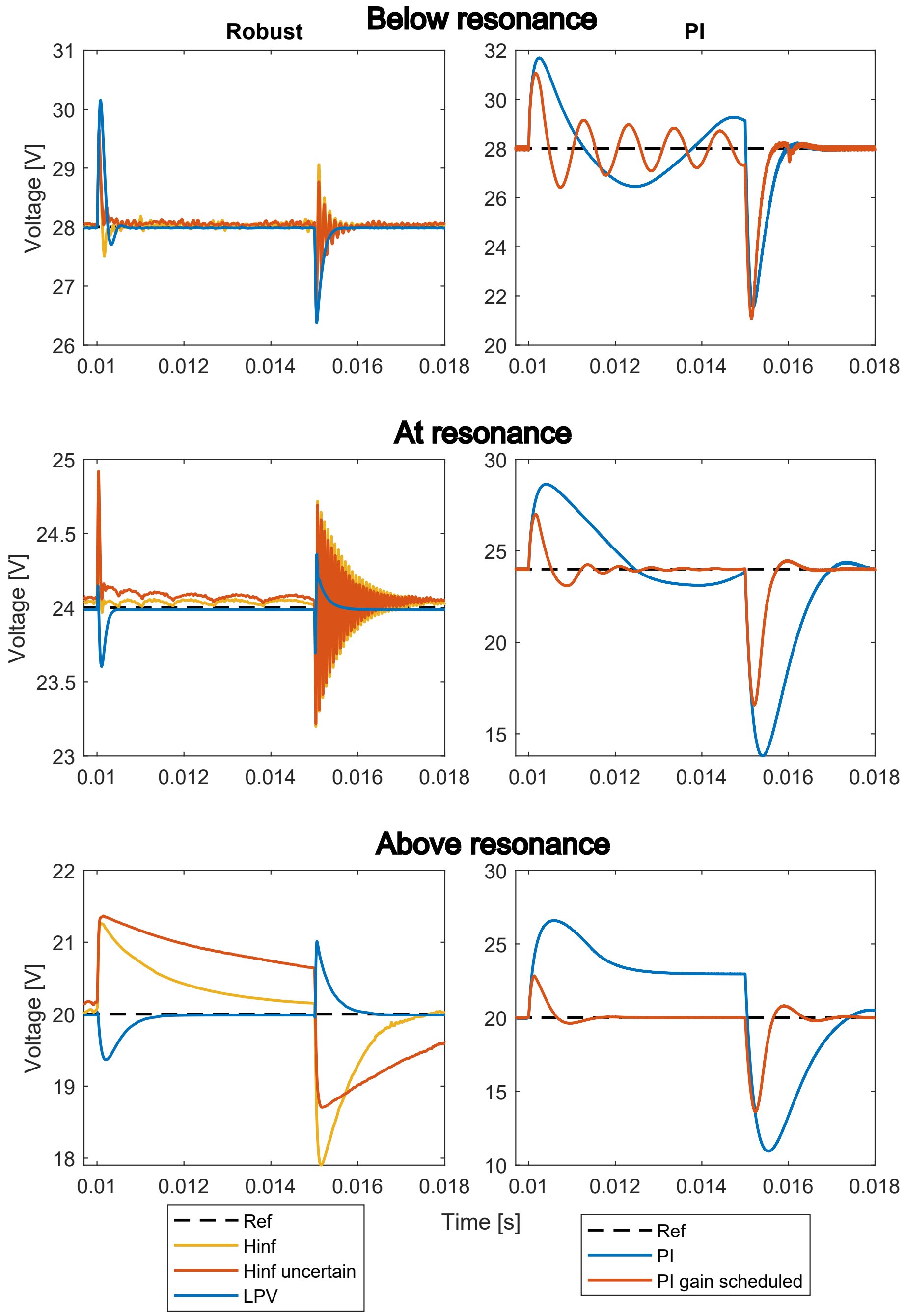

Figure 4.4: Load disturbance rejection for perturbed plant.

Overshoot and recovery time metrics were excluded this time, as the controllers showed practically the same behavior as in the nominal case. However, some differences were observed in the case of the LPV controller. The LPV controller now overcompensates in response to load steps, this is particularly noticeable at resonance and above resonance where it results in an undershoot instead for the first step.

4.3.2 Input disturbance

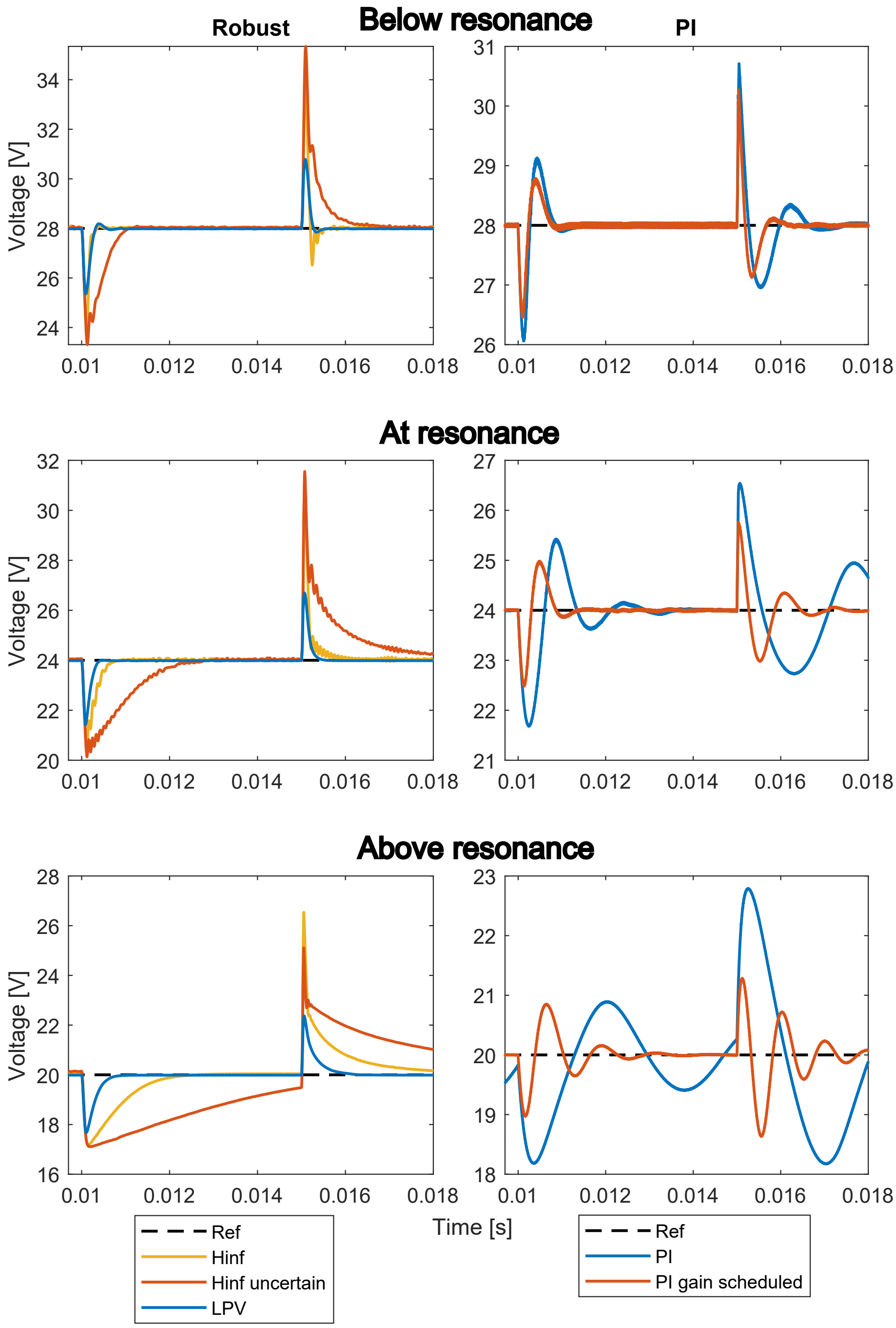

Figure 4.5: Input disturbance rejection for perturbed plant.

For the input disturbance case, the $\mathcal{H}_\infty$ controller was now stable below resonance, unlike the nominal plant. Apart from that, there were minimal variations in the behavior of the controllers, with very minor differences in overshoot and recovery times.

5 Discussion

5.1 PI

As observed from the results, the PI controller performed very poorly compared to the other controllers in most test cases. The simple PI structure with static gains is incapable of handling the whole operating range. As seen in Fig 4.2, the overshoots are very large, and large oscillations occur before settling. Clearly, the proportional term is insufficient to suppress the disturbances, causing large errors that are accumulated by the integral term (integral windup). Therefore, the design of PI controllers for LLC converters requires consideration of anti-windup and saturation methods for proper operation.

5.2 Gain scheduled PI

The gain scheduled PI controller solved the integral windup issue to some extent by scheduling the gains. Thus, the proportional gain can be varied throughout the operating range to better suppress disturbances, allowing the integral term to mostly accumulate only stationary errors. The improvement from gain scheduling is particularly noticeable for load disturbances above resonance. In this operating region, the system is overdamped with a lower voltage gain. Therefore, higher control effort is required. The gain scheduled controller can account for this by varying the gains. However, the below resonance region was still challenging for the controller. In this region, the system has a much higher voltage gain, requiring the gains to be more conservative. This suggests that the gain characteristics for the modified model may not be fully accurate in this region.

5.3 $\mathcal{H}_\infty$ & Uncertain $\mathcal{H}_\infty$

Both $\mathcal{H}_\infty$ controllers demonstrated improved load disturbance rejection and stability compared to the PI controllers across a wider operating range. However, the controllers still exhibited oscillatory behavior even at the nominal operating point, suggesting the need for further tuning. The nominal and uncertain variants performed similarly with some differences below and above resonance. The uncertain controller was tuned more conservatively to account for the specified uncertainty. Therefore, it displayed better performance in the below resonance region, where the voltage gain is much higher. However, this caused the uncertain controller to be overly conservative in the above resonance region. Conversely, the less conservative nominal controller exhibited the opposite behavior, showing improved performance above resonance but worse below resonance.

The input disturbance rejection capabilities were relatively worse compared to the PI controllers. This can be attributed to the generalized plant formulation, which does not describe the input disturbance. The state-space model used assumes a constant input voltage. Modifying the model to include the input disturbance as an input and thus allowing the controller synthesis to account for it could likely improve the input disturbance rejection.

5.4 LPV

The LPV controller was the superior controller among all the controllers evaluated. It consistently achieved the best performance in terms of disturbance rejection, overshoot, and settling time for most test cases. Additionally, it was the only controller without an oscillatory response to disturbances. The LPV controller was able to handle the varying voltage gains and dynamics across the entire operating range. It outperformed both the PI and $\mathcal{H}_\infty$ controllers in load disturbance rejection, making it a promising choice for LLC converters. However, as discussed previously with the $\mathcal{H}_\infty$ controllers, the LPV controller showed relatively worse performance for input disturbances due to the model structure.

5.5 Perturbed plant

The perturbed plant was specified as the nominal model with a 50% inductance loss and 10% capacitance loss. The main effect of this is a forward shift of the operating regions (switching frequency). To achieve the same output voltages, the converter had to operate at a higher frequency. The effects were negligible for most controllers except the LPV controller. As observed in Fig 4.4, the LPV controller overcompensates for load steps, resulting in an undershoot instead. The scheduling signal f_s is used with the wrong assumptions, as the controller is designed with the nominal model. Consequently, the LPV controller assumes a higher damping and lower voltage gain (above resonance) compared to the actual system, leading to aggressive gains and overcompensation of load steps. Despite this behavior, the controller still managed to outperform the other controllers for the perturbed plant.

This behavior was not observed for the gain scheduled PI controller, possibly indicating that the simple structure of the PI controller was unable to fully make use of the parameter variation described in the LPV model.

6
Conclusion

6.1 Summary

This project evaluated different controller strategies for a resonant LLC converter, ranging from the classical PI controllers to more robust model-based methods. The PI controller was unable to handle the varying voltage gains and dynamics of the converter. The gain scheduled PI controller showed substantial improvements by adjusting the gains throughout the operating range. However, it still encountered difficulties when operating below resonance.

The $\mathcal{H}_\infty$ controllers showcased improved disturbance rejection over the PI controllers but suboptimal response times for certain operating regions as the variation in dynamics was too large for the static gain controllers to handle. This further emphasizes the importance of a scheduled controller approach. In contrast, the LPV controller managed to handle the entire operating range while maintaining fast response times. The robust controller framework combined with a scheduled approach made the LPV controller a very effective and promising control method for future work.

6.2 Future work

There are a lot of aspects to further explore with the scheduled controllers. One interesting aspect is that the scheduling signal R_L is also the output disturbance of the system. Thus, it is possible to utilize it not only for scheduling but also as a measured disturbance input, which can further improve load disturbance rejection. This can be incorporated as an additional input to the controller or with a separate feedforward block.

An additional aspect to explore is state estimation for the scheduling signals. The current scheduling signals are assumed to be measured, requiring additional sensors for a practical implementation. However, it is possible for the scheduling signals to be estimated from observed outputs to reduce the sensor count.

The practical implementation of the controllers can also be explored. By investigating discretization, sampling time, and computational load, further insights can be gained regarding the practical applicability of the controller.

Bibliography

[1] F. Degioanni, I. G. Zurbriggen, and M. Ordonez, “Dual-loop controller for llc resonant converters using an average equivalent model,” *IEEE Transactions on Power Electronics*, vol. 33, no. 11, pp. 9875–9889, 2018.

[2] Infineon Technologies AG, *Resonant LLC Converter: Operation and Design*, 9 2012. Rev. 1.0.

[3] T. Glad and L. Ljung, *Control Theory*. Control Engineering, Taylor & Francis, 2000.

[4] R. Mallik, A. Jain, and S. Kapat, “A practical and cost effective wide range 6kw llc converter for ev charging infrastructure,” in *2023 IEEE Applied Power Electronics Conference and Exposition (APEC)*, pp. 2187–2193, 2023.

[5] S. Gao and Z. Zhao, “Magnetic integrated llc resonant converter based on independent inductance winding,” *IEEE Access*, vol. PP, pp. 1–1, 12 2020.

[6] C.-H. Chang, E.-C. Chang, C.-A. Cheng, H.-L. Cheng, and S.-C. Lin, “Small signal modeling of llc resonant converters based on extended describing function,” in *2012 International Symposium on Computer, Consumer and Control*, pp. 365–368, 2012.

[7] H. Khalil, *Nonlinear Systems*. Always learning, Pearson Education Limited, 2013.

[8] S. Kou and K. Han, “Limitations of the describing function method,” *IEEE Transactions on Automatic Control*, vol. 20, no. 2, pp. 291–292, 1975.

[9] K. Åström and T. Hägglund, *PID Controllers: Theory, Design, and Tuning*. ISA - The Instrumentation, Systems and Automation Society, 1995.

[10] S. Skogestad and I. Postlethwaite, *Multivariable feedback control: Analysis and Design*. Hoboken, US-NJ: John Wiley, 2005.

[11] A. Hjartarson, P. Seiler, and A. Packard, “Lpvtools: A toolbox for modeling, analysis, and synthesis of parameter varying control systems,” *IFAC-PapersOnLine*, vol. 48, no. 26, pp. 139–145, 2015. 1st IFAC Workshop on Linear Parameter Varying Systems LPVS 2015.

[12] L. Fortuna and M. Frasca, *Optimal and Robust Control: Advanced Topics with MATLAB®*. Taylor & Francis, 2012.

[13] S. Tian, F. C. Lee, and Q. Li, “Equivalent circuit modeling of llc resonant converter,” in *2016 IEEE Applied Power Electronics Conference and Exposition (APEC)*, pp. 1608–1615, 2016.

[14] D. Cittanti, M. Gregorio, E. Vico, F. Mandrile, E. Armando, and R. Bojoi, “High-performance digital multiloop control of llc resonant converters for ev fast charging with lut-based feedforward and adaptive gain,” *IEEE Transactions on Industry Applications*, vol. 58, no. 5, pp. 6266–6285, 2022.

[15] M. Mohammadi, F. Degioanni, M. Mahdavi, and M. Ordonez, “Small-signal modeling of llc converters using homopolarity cycle,” *IEEE Transactions on Power Electronics*, vol. 35, no. 4, pp. 4076–4093, 2020.

[16] MathWorks, *Designing Cascade Control System with PI Controllers*, 2023.

[17] Texas Instruments, *Understanding the Terms and Definitions of LDO Voltage Regulators*, 10 1999. Rev. 1.0.

[18] P. Mach and M. Horák, “Analysis of changes due to long-term thermal aging in capacitors manufactured from polypropylene film,” in *2020 43rd International Spring Seminar on Electronics Technology (ISSE)*, pp. 1–5, 2020.

[19] J. Kaiser and T. Dürbaum, “An overview of saturable inductors: Applications to power supplies,” *IEEE Transactions on Power Electronics*, vol. 36, no. 9, pp. 10766–10775, 2021.

DEPARTMENT OF ELECTRICAL ENGINEERING
CHALMERS UNIVERSITY OF TECHNOLOGY
Gothenburg, Sweden
www.chalmers.se

CHALMERS
UNIVERSITY OF TECHNOLOGY